Controls of Pre-existing Structures on Clinoform Architecture and the Associated Progradational System Elements

Roberto Clairmont[1*], Folarin Kolawole[1], Abah P. Omale[2], Heather Bedle[1]

[1]School of Geology and Geophysics, University of Oklahoma, 100 East Boyd Street, RM 710, Norman, OK 73019, U.S.A.
[2]Department of Geology & Geophysics, Louisiana State University, E235 Howe Russell Kniffen, Baton Rouge, LA 70803, U.S.A.
**Corresponding author: roberto.d.clairmont-1@ou.edu*

Abstract

There remains a limited understanding of the controls of preexisting structures on the architecture of deep-water progradational sequences. In the Northern Taranaki Basin (NTB), New Zealand, Pliocene post-extensional sedimentary sequences overlie Miocene back-arc volcaniclastic units. We utilize seismic reflection datasets to investigate the relationships between the buried back-arc mound-shaped structures, and the spatio-temporal changes in clinoform architecture and the associated progradational system elements within the overlying continental slope margin sequences. Our results reveal: (1.) buried mound shape structures in the northern domain of the study area, overlain by younging progression of shelf-to-basin prograding clinoforms; (2.) folding of the deeper clinoforms that systematically decrease in magnitude with shallowing depth from the top of the seamounts; (3.) overall, the N-S-trending continental slope margin evolves from a highly curvilinear/angular trend in the deeper clinoforms (Units 1-2) into a rectilinear geometry within the shallower post-extensional intervals (Unit-3 and shallower); (4.) Units 1-2 characterized by dominance of stacked offlap breaks and over-steepened (7-10°) clinoform foreset slopes in the northern domain, and dominance of gently dipping foreset slopes (<6°) in the south; (5.) Unit-3 show very low (<5°) and intermediate (5-7°) foreset slopes across the entire survey; (6.) in the northern domain, differential loading by prograding sequences about the buried seamounts and horst-graben structures induced a differential compaction of the deeper units, which influenced a temporal pinning of the prograding slope margin in pre- Unit-2 times; and (7.) wide, closely-spaced channel incision into over-steepened slopes dominate the deeper prograding sequence in the northern domain, whereas, narrower, straighter channels dominate the south. We show that the buried preexisting structures constitute rigid buttresses that modulated the syn-depositional topography and post-depositional architecture of the prograding sequences in the NTB. Our findings present a distinction in the controls on progradational sedimentation patterns between magmatic and non-magmatic continental margins.

Keywords: Clinoforms, Sedimentation patterns, Paleovolcanoes, Deepwater, Extensional margins, Shelf-margin, Igneous-structures

1 INTRODUCTION

Few studies have intensively explored the potential link between buried structural features and their influence on subsequent sedimentary sequences (Hardage et al., 1996; Tsikalas, et al., 1998; Anka et al., 2009; Alves, 2010; Johnston et al., 2010). This leaves much in question as to the influence of pre-existing structures on the basinal sedimentation patterns associated with eustatic sea level changes, climate, and tectonic-related events. The purpose of this study is to examine how inherited paleovolcanic edifices alter the architectural elements, geometry and other large-scale features of the overlying, prograding strata (clinoform packages). Several studies have analyzed the intricate internal architecture, depositional sequences, and potential economic significance of clinoforms (e.g., Hansen and Kamp, 2006; Berton et al., 2016; Salazar et al., 2016). However, the controls of inherited tectonic structures on clinoform architecture remain a longstanding problem.

Clinoforms encompass multi-scale (tens of meters to kilometers) sloping depositional surfaces that are associated with the progradation of sediments in deltaic environments and continental shelf settings (Mitchum, 1977; Patruno and Helland-Hansen, 2018). Due to the regionally extensive nature of continental-shelf margins, clinoforms provide a great opportunity to pin-point the salient features that potentially indicate the influences of buried structural features. Three distinct geometrical sections that characterize a clinoform package include topsets, foresets and bottomsets, describing their erosional and depositional basin-ward structure. Progradational system elements are largely controlled by sediment supply, however, eustatic sea level changes and tectonism may influence the associated sedimentation patterns and therefore the shape of clinoform profiles (e.g., Emery and Myers, 1996).

Buried structural features may influence the morphology of the earth's surface and the associated sedimentation processes (e.g., Gomes et al., 2014; Mortimer et al., 2016). Many studies implicate that igneous activities may deform the shallow crust and modify the surface morphology at the time of emplacement (e.g., Bridgwater et al., 1974; Feuillet et al., 2002; Hansen and Cartwright, 2006; Muirhead et al., 2012; Holford et al., 2012; Jackson et al., 2013; Magee et al., 2016, 2018; Reynolds et al., 2018; Kolawole et al., 2020). Post-emplacement, igneous edifices may influence seabed sedimentation, and local distribution of crustal load and geometry of the subsequent sedimentary successions (e.g., Infante-Paez and Marfurt, 2017; Infante-Paez, 2018; Jackson et al., 2019).

In the northernmost Taranaki Basin, New Zealand (Figures 1a-c), shallower Early Pliocene sedimentary sequences are characterized by an excellent stacked succession of laterally outbuilding sequences that overlie Middle to Late Miocene back-arc extension volcaniclastic sequences, Mohakatino Volcanic Complex (Stagpoole and Nicol, 2008; Giba et al., 2010, 2013). The region of the volcanic edifices, observed in seismic reflection data along the western continental shelf of the North Island (Giba et al., 2013), provide an excellent location to explore the influence of the igneous structures on the geometry of the migrating shelf margin and therefore clinoform sequence stratigraphy and the associated progradational system elements.

In this study, we utilize seismic reflection datasets to analyze the spatio-temporal variations in the architecture of the post-extension progradational sequences that overlie inherited syn-back-arc extension seamounts. We show that in this region of the Taranaki Basin, differential loading by the overriding clinoform sequences about buried seamounts and horst-graben structures induced a differential compaction of the deeper units which modulated the syn-depositional location and geometry of the deeper clinoform sequence boundaries, and post-depositional geometries of the clinoform packages. Further, our findings present a distinction in the controls on progradational sedimentation patterns between magmatic and non-magmatic continental margins (both convergent and divergent).

2 GEOLOGICAL SETTING

2.1 Pre- Middle Miocene

The Taranaki Basin evolved as a rift basin during the Late Cretaceous as the New Zealand continent separated from Gondwanaland (Stagpoole et al., 2001), and continued to experience extension up till the Late Paleocene (Palmer, 1985). It formed as a result of the subduction of the Pacific Plate beneath the Australian Plate about ~40 myr ago (Giba et al., 2013; Stagpoole and Nicol, 2008; Seebeck et al., 2014), where both plates converge at the Hikurangi Trough (See Figure 1a inset), which runs south to north, toward the eastern end of the island (Giba et al., 2010). The Hikurangi subduction margin initially had a NW-SE trend (Giba et al 2013; King, 2000) eventually orienting to a NE-SW trend. The basin is situated on the overriding Australian Plate and is located on the western coast of the North Island (Figure 1a), is approximately 60km wide and extends for about 350 km in a NNE direction from the south Taranaki Peninsula to the offshore coast, west of Auckland (Giba et al., 2010). The structure of the basin is separated into two main components, the Western Stable Platform and the Eastern Mobile Belt (King and Thrasher, 1996) and is non-distinctly bounded by the Northland Basin to the north and the Deepwater Taranaki Basin to the west.

In the Oligocene to Early Miocene period, the Hikurangi subduction margin, which began to develop between the convergent event of the Pacific and Australian plates (Uruski and Baillie, 2004), caused the Taranaki Basin to transition from an extensional tectonic setting into a contractional tectonic domain (King, 2000). Primarily, a 50-degree rotation, about a vertical axis, of the Australian Plate (~24 myr) was accompanied by steepening of the westerly subducting Pacific Plate (Giba et al., 2010, 2013; Kamp, 1984). This clockwise vertical rotation of the North Island, of New Zealand, was then followed by north and west extension and south and east shortening of the Australian plate (Giba et al., 2013; Nicol et al. 2007). The northern region of the basin then witnessed the development of andesitic volcanism and intra-arc/back-arc extension in Early Miocene, corresponding to the subduction (Stagpoole et al., 2001, Herzer 1995). This is a result of dehydration of the westward subduction Pacific Plate (Seebeck, 2012; Bischoff et al., 2017) and/or partial melting of the plate (King, 2000). This magmatic event led to the emplacement of the NNE-SSW-trending Mohakatino Volcanic Belt (MVB) in the northern Taranaki Basin (Figures 1a and 1c), consisting of mainly submarine volcanic centers (Giba et al., 2010 and 2013; Seebeck, 2012). Additionally, the MVB has over 20 volcanic centers, covering an area of ca. 3200km^2 (Lodwick et al., 2019), stretching a distance of about 200km, from the northern coastal area of the Taranaki Peninsula (See Figure 1a).

2.2 Late Miocene - Early Pliocene

Late Miocene to Pliocene activity in much of the Northern Taranaki Basin involved back-arc extension tectonics associated with the Hikurangi subduction zone of the Australian-Pacific plate margins. Extensional faulting within the basin formed a c. 40km wide depocenter, known as the Northern Taranaki Graben (Hansen and Kamp, 2004a, 2004b), bordered between the Turi Fault Zone and Cape Egmont Fault Zone (Stagpoole et al., 2001). The graben occupies an area of 10,000 km^2. Hansen and Kamp (2004a) observed Late Miocene to early Pliocene stratigraphic units formed deep within the structural formation of a Northern Graben and below the onset of the Giant Foresets Formation (GFF). These stratigraphic units have been characterized as the Ariki Formation and the Early Pliocene basin floor fan of the Mangaa Formation, respectively (Hansen and Kamp, 2004a). The Ariki Formation is a marly condensed interval related to the starvation of terrigenous sediment to the northern parts of the basin and the Mangaa Formation is a thick sandstone-dominated unit (Hansen and Kamp, 2002, 2004a). The structural limits of the Northern Graben and its continuing extension affected the depositional environment during local chronostratigraphic stages of the Waipipian (3.5 – 2.79 Ma) to Mangapanian (2.79-2.28 Ma), in early Pliocene; together with the existence of volcanic massifs of the Mohakatino Formation that influenced the way the paleogeography would affect siliciclastic sediment accumulation (Hansen and Kamp, 2002, 2004b).

2.3 Middle Pliocene to Recent

In the late local chronostratigraphic stage of the Nukumaruan (1.8 – 0.33 Ma), structural influence of the graben maintained and aligned the deposition of material in a sloping SE to NW direction, with little impact of subsidence on sedimentation (Hansen and Kamp, 2004a). Substantial voluminous sediment was then supplied to the adjacent sedimentary basins, as the southwest-dipping subduction zone of the northern region of New Zealand uplifted and exposed parts of Zealandia in the Neogene (Nicol et al., 2007; Bischoff et al., 2017). The source of the deposited sediment supply would be derived from the uplifted Southern Alps created <8 Myr ago (Tippet and Kamp, 1995). In the Pliocene and Pleistocene, the Taranaki basin would then be filled with sediment associated with the Giant Foresets Formation, which prograded at rapid rates in a north and predominantly westward direction, building onto the undisturbed Western Stable Platform (Giba et al., 2010, 2013; Stagpoole et al., 2001) as the rate of uplift increased. This sequence of sedimentation filled the Northern Taranaki Graben with a thick succession of deep-water sediments (Bischoff et al., 2017) and continued to bury the Miocene aged MVB volcanic seamounts (Stagpoole et al., 2001) within the last ~20 myr. Thicker units of the GFF would be expected within the graben, due to subsidence and syn-sedimentary tectonics (Hansen and Kamp, 2004a). Additionally, the GFF is predominantly characterized by low-angle shelf-edge trajectories (Anell and Midtkandal, 2017). This regional formation is the result of rapid progradation and aggradation of late-early Pliocene to relatively recent succession of the continental margin that underlies the modern shelf-to-basin ward structure (Hansen and Kamp, 2002).

Seismic interpretation studies reveal the varying litho-facies and geometrical elements of the GFF. Its top-sets are indicative of coarser grained sandstone and muddy siltstone; the foresets include an accumulation of fine-grained mudstone and muddy siltstone, with variability in its lithology along the degradational surface and the bottom-sets are described as being composed of either sandstone or mudstone (Hansen and Kamp, 2002). The observation of the GFF in seismic data reveal no distinct geological boundary northward, into the southern part of the Northland Basin. Johnston (2010) have provided potential evidence of progradational successions in the southern region of the Northlands basin due to growth of the shelf margin in the Pliocene that overlay the buried volcanic massifs.

3 DATA AND METHODS

3.1 Seismic survey and well data

To address the onset and evolution of the progradational events including the GFF, the 3-D Nimitz survey was selected for analysis. The survey which was acquired by the Swire Pacific Offshore owned vessel, Pacific Titan, was operated by Compagnie Générale de Géophysique (CGG) from January through April 2007. It is located along the western coast of the North Island New Zealand (Figure 1a) covers approximately 432 km^2 and provides a recording length of 6500 ms (O'Leary et al., 2010). Inline and crossline interval dimensions are measured at 25 meters and 12.5 meters, respectively. The data has SEG positive display polarity, correlating impedance increases with positive amplitude reflection and the recorded sampling rate is 2 ms. Quality Control (QC) processing was conducted to determine issues associated with acquisition and recording for every line and to determine the impact of noise on the data. For example, a bulk shift static correction was applied to the seismic data to correct for a 50 ms delay in instrument recording, true amplitude recovery was applied using a spherical divergence correction, band pass filtering was also performed, followed by NMO (Normal-Moveout) and stacking (O'Leary et al., 2010).

Prior to seismic interpretation, we utilized the Korimako-1 well (Figure 1b) to perform the seismic-to-well tie and complete a time to depth conversion of the seismic dataset. We tie the well to the seismic to get the interval velocities, and using the interpreted horizons and well-log velocity information, created a P-wave model. The P-wave interval velocity model was then used to convert the seismic to depth. Time-depth curves from sonic data used to create the synthetic seismograms (O'Leary et al., 2010) indicate an average velocity of 1710m/s from the top of the log at 454.6 m and a Mean Sea Level (MSL) datum. Given that we observe a dominant seismic frequency of approximately 20 Hz, this provides vertical (1/4 wavelength) resolution of ~21m.

As a wildcat exploration well, its intended goal was to target sands similar to the Miocene Mangaa Formation. Drilling of the Korimako-1 well dated between October-November 2010, and reached a maximum penetration depth of 1946 m. Unfortunately, the well turned out to show no significant economic impact, and was therefore abandoned. The results revealed high risk AVO (Amplitude versus offset) and amplitude anomalous targets within the Pliocene-Miocene strata linked to differences in the properties of shale, mistaken for potential reservoirs. We utilize stratigraphic markers and the associated ages from the Korimako-1 well-completion reports (O'Leary et al., 2010) to aid in constraining the ages of major stratigraphic surfaces in the survey.

3.2 Seismic interpretation methods

We use conventional seismic data interpretation techniques and 3-D seismic attributes to investigate the geological features in the 3-D Nimitz survey. Although seismic resolution of the seismic acquisition provides ~5 TWTs of seismic imaging, seismic interpretation was limited to the seismic reflection data above 1.6 TWTs in addition to the underlying dome-shaped structures just below 1.6 TWTs. Herein, we use the terms "clinoforms" and "clinothems" respectively as chronostratigraphic horizons (surfaces traced by single amplitude reflectors) and the deposited features contained by these surfaces (Slingerland et al., 2008). We delineate the clinothems (clinoform packages) using continuous high-impedance reflectors in a shelf-to-basinward direction similar to published approaches (Anell and Midtkandal, 2017; Gomis-Cartesio et al., 2018). We utilize standard seismic facies analyses techniques (Berton and Vesely, 2016) and simple seismic stratigraphic terminology (Vail, 1987; Steel and Olsen, 2002) to interpret the clinothems, their architectural elements, and the associated progradational system elements. A two-dimensional (2-D) seismic transect (CNL95B-38) line is also included to indicate the regional extent of the studied GFF (See Figures 1a and 2a, S1).

We use a bottom-up approach in our structural and stratigraphic mapping. First, we map the reflector bounding a deep-seated buried mound-shaped feature in the survey. Afterward, we map four strongly basin-ward-dipping, high impedance reflectors (R1 to R4). These reflectors bound packages of the same geometries (U1 to U3), (Figures 2b and 2c). Moreover, the reflectors, observed as the clinoform surfaces were mapped throughout the 3-D volume. We use these surfaces as key horizons delineating the regional changes in pale-topography and clinoform architecture from north to south across the survey. To better understand temporal evolution of the geometry and location of these key surfaces, as the extents of coverage of our dataset allow, we quantify the maximum foreset dip angle or "maximum foreset angle" (Figure 3a), and the location of the toe of the continental slope/top of the continental rise (Figure 3b), herein used as the "toe-of-slope inflection point". The former indicates the maximum angle measured along the clinoform surface in the foreset region, while the latter indicates the first noticeable change in angle upslope (i.e base of the slope). O'Grady and Syvitski (2002) define the base of the slope as a point in which there is a significant decrease in the dip of the slope, which can be generally difficult to define due to less dramatic changes and inconsistency along the lower margins. Additionally, the continental rise has been defined as a uniform gentle sloping surface that lies at the base of the continental slope, in the absence of trenches (Heezen et al., 1996), on which mainly terrigenous sediment is deposited at high rates (Heezen et al., 1996; Murdmaa et al., 2012). We take these two measurements along five profile transects spaced 6 km apart (L1-L5).

We compute standard 3-D seismic attributes and surface-extracted displays to map the sedimentary dispersal features (e.g., channels, mass transport deposits etc.) along the mapped dipping reflectors. More specifically, we use the structural curvature, variance (coherence), and root-mean-square (rms) amplitude seismic attributes. Curvature is the 2D second-order derivative of both the inline and crossline components of the calculated dip; hence structural curvature is the 2D second-order derivation of the structural component of the reflections along vertical seismic (Chopra and Marfurt, 2013). It is particularly useful in identifying and constraining channel geometries, faults and fracture intensities. Variance is an edge detection method that uses local variance as a measure of unconformity in signal traces (Randen et al., 2001). The Variance attribute is used to identify fault trends and discontinuities in the seismic character derived from potential erosional features. Root-mean-square (RMS) amplitude is the square root of the sum of the square of amplitude values within a window length (Chen and Sidney, 1997; Chopra and Marfurt 2008). RMS amplitude aids in interpretation since it can differentiate areas with changes in acoustic impedance associated with lithological variations such as fluid content, and sand and shale contrasts in siliciclastic regions (Amonpantang et al., 2019). It is therefore useful in revealing channel morphologies (Amonpantang et al., 2019), basin floor fans, and depositional features such as mass transport deposits, slump deposits and shale drapes/debris flow (Gong et al., 2011). Lastly, due to the dipping foreset successions and lack of clear reflections within the clinothems in the Nimitz 3D dataset, we apply the stratal slicing method to explore the spatio-temporal evolution of the analyzed stratigraphic units (Figure 2c). Using two non-parallel dipping clinoform surfaces, a total of nine (9) stratal slices within each unit were generated and investigated (Figure 2c).

3.3 Modelling of stratigraphic decompaction

Further, to better understand the influences of deeper rigid blocks (e.g., buried volcanic edifices) on the overlying clinoform geometries and architecture, we investigate the role of differential compaction on the 2-D spatio-temporal distribution of lithologic unit thicknesses. To evaluate the timing and magnitude of differential compaction about the buried volcanoes, we carry out 2-D decompaction on six layers identified within a representative seismic cross-section in the northern part of the survey. Decompaction reverses the porosity loss and reduced thickness caused by the weight of overlying sediments on a buried layer. Standard decompaction steps involve the removal of the topmost layer and allowing all the layers below to expand back to their thickness prior to the deposition of the removed layer. Porosity loss during burial depends on lithology and is assumed to follow the exponential relationship shown in Table 1 (Allen and Allen, 2006; Sclater and Christie, 1980). We use compaction parameters calculated for the Taranaki Basin from best-fit porosity-depth curves of compensated formation density-determined porosity (Table 1) (Armstrong et al., 1998). We use the flexural decompaction software ‘FlexDecomp’ (Badley’s Geoscience Ltd) for the decompaction exercise.

$$\Phi=\Phi_0 \, e^{-cz}$$

Φ= Porosity at depth (%)
$\Phi 0$ = Porosity at the surface (%)
c= porosity-depth coefficient (km^{-1})
z= depth

The removal of sedimentary layers may result in an isostatic uplift of the basement because of mechanical unloading. However, we assume that this effect is insignificant in our study depth intervals. Therefore, we focus solely on the decompaction of the layers by keeping the basement at a fixed depth throughout the decompaction iterations.

Table 1. Parameters used for decompaction

Layer	Surface porosity Φ_0 (%)*	Porosity-depth coefficient (km^{-1})*
1	50	0.44
2	50	0.44
3	50	0.44
4	50	0.44
5	50	0.44
6	50	0.44

*Armstrong et al. (1998)

4 RESULTS

The subsurface structure of the study area (Figures 4a-c) consists of a deep (850 – 2500 TWTms) syn- back-arc extension interval where pervasive normal faulting dominates, overlain by a transition phase (500 – 850 TWT ms) and a post-extension section (<500 TWTms) that largely consists of prograding clinoform packages. We group the clinoform packages into three units, Unit-1 to -2 (transition phase) and Unit-3 (post-extension phase) and are bounded by surfaces R1 to R4 (Figures 2b and 4a-4c). Below, we describe the relevant features of each of these intervals.

4.1 Deep-seated dome-shaped mega-structures

Within the syn- back-arc extension section, we identify dome-shaped features in the seismic dataset (Figures 4a and 5a-b). The dome-shaped structures are all located in the northern domain of the seismic volume, within which one dome sits at the northernmost edge of the survey, and another to its southeast (V1 and V2 in Figure 1b). A strong, bright, positive reflector defines the upper boundary of the dome features (R_0 reflector in Figure 5b) which peaks at 1000 - 1250 TWTms. The largest of the two domes (V1) has a diameter of ~6.2 km, measured at the largest inflection point toward its base. Its internal character is mostly chaotic, mid-low amplitude responses that lack strong continuous reflectors, sustaining at deeper depths below the dome structure (Figure 5b). Within the chaotic zone, we observe the presence of short high amplitude 'saucer-shaped' features and several low-amplitude reflectors that extend steeply upward into the central axis of the mound (Figure 5b). We identify multiple cone-shaped features along the lower slopes of the mound (Figure 5b). On the flanks of the dome structures, gently- to steeply-dipping reflectors onlap onto the strong, bright positive reflector, as well as steep normal fault segments that cut downwards into the dome structures. Above the dome-shaped features, the succeeding stratigraphic units show folding that systematically decrease (log-linear trend) in magnitude with shallowing depth from the top of the dome features (Figures 5b and inset).

4.2 Clinoform sequence boundaries

The Korimako-1 well markers constrain surface R1 to be of Mid Pliocene age, surface R2 to be a unit at ~20 ms above the Top Pliocene, likely the base of the GFF, surface R3 to be somewhat Early-Mid Pleistocene, and surface R4 defining the top of the GFF (O'Leary et al., 2010). For simplicity we use these four horizons (clinoform surfaces) to divide the clinothems into units U1, U2, and U3 (Figures 2b and 2c). Figure 2a reveals the full extent of the GFF, initiating at the oldest shelf-edge location and a generally continuous trend in outbuilding geometry, although some interpreted faulting occurred thereafter. The vertical seismic sections, relatively closer to the modern-day continental shelf (Figures 4b-c, see inset on 4a for location) show the variations in the thicknesses of the three depositional units bounded by the reflectors. Surfaces R1 and R2 bound the first succession, Unit 1 (U1), whilst

Unit 2 (U2) is bounded by R2 and R3. As observed in the seismic section (Figure 4c), here, surfaces R3 and R4 bound the facies along the continental shelf or topset region of the clinoform package labeled as Unit 3 (U3). The Mangaa Formation represents the bottomsets of the GFF, and as such are observed in the southern domain of the seismic section, as compared to the northern domain, where we see the upslope, foreset seismic facies. As a result, Figure 4c shows the foresets of U1 in the northern domain, and these basinward ‘bottomsets’ toward the southern domain, and U2 highlights most of the foreset seismic facies of the prograding clinothems from the central to southern domain of the seismic survey. Overall, as we navigate northwest across the seismic survey, toward the basin, we will observe at best, topset, foreset and bottomset (e.g., southern domain of U1, Figure 4a) seismic facies for each defined unit, along northern, central and southern domains of the survey.

The mapped surfaces (Figure 4c) reveal a northward thinning of Unit 2 with an abrupt lateral increase in the angle of the R2 surface at the middle of the transect. Consequently, the thickness of Unit 1 decreases from approximately 460 TWTms in the northern domain to 174 TWTms in the central region of the study area and increases again to about 274 ms TWT in the south. There is apparently no seismic facies consistent with foreset geometries within Unit 1 toward the south. Additionally, in the north, Unit 1 consists predominantly of V and U-shaped, continuous high amplitude reflectors that incise vertically into the underlying strata. These reflectors are “truncated” toward the south, by the surface R2. The thinner central domain of Unit 1 consists of mostly continuous subparallel, high amplitude reflectors deformed by the underlying syn-depositional sequence and faults that terminate at the surface R2. Cross-sections reveal that the increase of the angle of the lateral trend of surface R2, together with the non-uniform thickness of Unit 1, can be due to the position of the seismic inlines slicing through a zone of the continental shelf in the north and more basinal settings toward the south. However, keep in mind that the non-uniform thickness is also influenced by the aforementioned, underlying syn-depositional sequence. This is a result of the layout and alignment of the acquired seismic volume along the New Zealand coast. We therefore see more available space of the northern graben depocenter in the southern domain, which is mainly influenced by this back-arc syn-rift sequence. This sets up the observed thickness of the next prograding clinothem, Unit 2 (U2).

The northernmost section of Unit 2 is approximately 74 ms TWT and thickens to about 488 ms TWT consistently throughout the southern sections of the inline cross section (Inline 1440, Figures 4b and 4c). It is composed predominantly of similar V and U-shaped wavy-subparallel, mid-high amplitude reflectors, less distinct as those observed within the thicker Unit 1 facies. They are also channel type features, potentially submarine gullies or smaller submarine canyons. Toward the basin, along inline 1225 (See Figure 4a, inset) located in the mid-sections of the 3D volume, we observe the more distal facies (lower slopes and bottomsets) of Units 1 and 2, and the foreset facies of Unit 3, dominated by mid-high amplitude, continuous wavy reflectors throughout most of the package (Figure 4a). The high frequency and timing of these features correlate to submarine gullies studied in the region of the Taranaki Basin (Shumaker et al., 2017). Additionally, we observe a north-dipping fault that extends from the deeper syn-rift sequences up into the shallower units (Fault D; Figure. 4a).

4.3 The geometries of the clinoform sequences

Normalization of the surfaces allowed us to observe the migration of the system by identifying the point at which there is an abrupt change in slope from the proximal basin floor to the distal foreset slope, or the toe-of-slope inflection point (See Figure 3). We use a formula, S_c+d_{Rx} (Figures 3b) to observe the lateral location of this inflection point. This formula represents the summation of the average distance of the eastern edge of the survey away from the western New Zealand coastline (S_c = ~38,800 meters) and the distance of the observed inflection point (i.e d_{Rx}) from the right edge of the seismic (See Figure 3b). The angle of the maximum foreset dips (Refer to Figure 3a) are taken along cross sections L1-L5 on the depth converted seismic volume to observe the variations in trends of dip along each clinoform surface. The spatial extent of the seismic from east to west does not allow us to measure the dip of the foreset along each surface on the seismic cross sections (eg. L1, across surface R1 – Figure 6a). Figures 2b and 2c shows the limited spatial extent along surface R1 for measuring the maximum foreset dip. In addition to the inflection points measured along the surfaces, we identify from the normalized surfaces, a unique trend used to qualitatively identify the shape of the continental slope margin. This was defined by an 80% max. depth contour line. This trending line, shows the older surfaces (R1 and R2) consisting of a predominantly curvilinear geometry, exaggerated in the south, to a more rectilinear geometry in the succeeding surfaces (figure 7).

The graph plots for cross sections L1, L2 and L4 (Figure 6a, 6b and 6d, reveal similar trends in the distance of the inflection point from the continental slope ($S_{xc}+d_R$) versus depth in two-way-travel time. Additionally, both plots of the L3 and L5 cross sections show another distinct trending style, compared to L1, L2 and L4. We describe each of these styles as Progradation Style A and Progradation Style B, respectively. Progradation style A indicates an initial steep upward trend of the observed inflection points, before an abrupt change to a downtrend. Progradation style B also shows an initial, steep upward trend, but experiences a less abrupt, gradually increasing trend. The tightly clustered points (Figure 6f) highlights the geometrical uniformity across the survey, following the trend of the toe-of-slope inflection point of the prograding system, on the more recent R4 surface whilst the most separated points describe the greatest geometrical non-uniformity along the older R2 surface (dashed line connecting points at R2 surface). The largest dip values are recorded in the north with maximum foreset dip angles at approximately 10° across section L1 on surface R2 (Figure 6a) and 8° across section L2 on surface R2 as well (Figure 6b). Along surface R3 the dip of the maximum foreset angles in the north decreases from ~7.5° (Figure 6a) to ~6.6° (Figure 6b), and as low as ~4.8 in the south (Figure 6e). Along surface R4 the maximum foreset dips decreased from ~7.9 in the north (Figure 6a) to ~6.8 (Figure 6b), to as low as

~4.° in the south. Generally, the mid-lower slope and basinward units of the system is observed along surface R1, whilst we are able to identify more low-to-upslope environments and eventually the upslope-to-shelf edge region of the clinoforms along surface R4. This however, varies along the regionally defined domains of the survey. With the deposition of each unit, the shelf-to-basin system generally migrates to the northwest without the buried mound features influencing the input of sediment, and progradation of the clinoforms in the younger units.

4.4 Internal architecture of clinoform packages

4.4.1 Unit 1 (U1) drainage network patterns

Proportional slicing produces a better interpretational approach of the internal architectural elements of each chronostratigraphic clinothem, compared to time-slice intersections. The nature of the clinoforms makes it difficult to accurately identify features along the dipping surfaces on the time-slice intersections. In addition to the steepness of the shelf-edge, deep-seated mound shape features in the north have influenced the progradational evolution of this earliest succession, such that structural highs of the region have resulted in large channels that migrate toward the basin, deeply incising into the shelf-edge and along the upper slopes (Figure 8). The northernmost dome-shaped feature has also directed sediment flow toward the southwest along the slopes of the deposited strata, indicated by the dashed arrow (See Figure 8b). Younger stratal slices (S8) within Unit 1 (Refer to Figure 2) potential canyon sized channels that have incised deeply (i.e. valley incisions ranging from 80-120 meters deep) into the underlying strata due to the steepening of the slopes likely influenced by differential compaction at lower sections of the U1 layer (Figure 9a). The widths of these deeply incising channels vary between 700-1100 meters. Though we identify channel or valley-like features along the proximal shelf-to-basin region, south of the curvature attribute surface (green arrows, Figure 9a), it does not reveal much distinct channel geometry toward the basin. This is likely due to complexity of horizon mapping or termination of the growth of channels in the zone indicated by the red arrows. Recall that due to the layout and areal limit of the seismic, specifically to the east, it is likely that these are identical to the "canyon sized" valleys we identify in the north (green arrows, Figure 9a) that flow basinward in the central and southern regions.

4.4.2 Unit 1 (U1) erosional and depositional features

Unique to this older clinoform package, is the nature of the attribute response (bounded by the polygon) with lateral margins trending primarily east-west, distinctly revealed along the generated variance surface (Figure 8c). This enclosed body consists of a mostly chaotic seismic character of high discontinuous variance zones, with globular low variance values. This mass of chaotic stratigraphic facies is also observed on the cross-section view as an interval of highly disrupted seismic facies of low-mid to mid-high acoustic impedance values (Figure 8a) that is enclosed by a basal shear surface and topped by parallel continuous, high amplitude reflectors. The thicker and thinner portions are potentially influenced by underlying half–graben and horst-block structures. Additionally, we observe that a ENE-trending fault extends up shallow and cuts the surface (Figures 4a and 9a-b).

4.4.3 Unit 2 (U2) drainage network patterns

Channel features continue to dominate the northern most region of this unit, as the mapped stratal slices sustains a topographic high primarily in the northern domain (Figures 10a-d). Channel width is smaller compared to the incising canyon-like valleys in the same area of the previous succession, however the central region of the attribute interpolated surfaces consists of more channels migrating as the clinoforms out-build and prograde basinward in a northwest/west direction (Figure 10a).

4.4.4 Unit 2 (U2) erosional and depositional features

Keeping within the confines of the central area of the stratal slice (S5), we observe a zone of wavy-like chaotic responses in negative structural curvature, likely to be either a detached slope fan unit or slump (Figure 10a). This erosional feature is better revealed along the variance attribute surface (Figure 10b). This is chronostratigraphically followed by low sinuous channels that gently meander toward the basin floor flowing through the eroded slope fan unit/slump feature along stratal slice S8 (Figure 10c). Additionally, in the younger sequences of this unit, along stratal slice S8, RMS amplitudes reveal a high positive response within the channel geometries (Figure 10d) and support the potential for the channels to consist of coarser grained sediment infill. Further analysis of the RMS amplitude stratal slice shows a high RMS oval-shaped feature toward the south enclosed by the black dotted line, similar to the geometry of a fan lobe deposit (See also Figure 10d). A linear channel-like feature with mid to high-mid RMS values joins the fan lobe from along the proximal slope but is not easily distinguished within the high RMS region.

4.4.5 Unit 3 (U3) drainage network patterns

The lateral extent of the seismic volume has constrained the interpretations of this unit along the continental shelf-edge to the upper sections of its lower slope. Since this unit consists of distinct seismic interpreted features consistent with studies (Hansen and Kamp, 2006; Salazar et al., 2016; Shumaker et al., 2017) in the central and southern explored Taranaki Basin's Giant Foresets Formation, we are able to compare our internal architectural findings with some of the previous work done on the GFF. The early onset of this succession is characterized by a dense network of linear channels that feed into the basin (Figure 11). Compared to the previous successions, the slopes of this unit are less steep, and there are no paleo-topographic or structural highs that allow for channels to incise deeply into underlying strata. There are also no erosional or depositional features observed along the generated stratal slice surfaces.

4.5 Stratigraphic decompaction models of the prograding units

We present the results of the sequential decompaction of the post-R4 units and Units U3 to U1 in Figures 12a-e. In iterations #1 (removal of Post-R4 units) and #2 (removal of Post-R3 units), the syn-depositional locations of the continental slope margin are to the west of the volcano, and there are no significant changes in the unit thicknesses and maximum foreset dip angles (Figures 12b-c). However, in iteration #3 (removal of Post-R2 units; Figure 12d), we observe that the continental slope margin is significantly narrower, and the associated maximum foreset angle is steeper than those of Time R3 (in iteration #2) and Time R4 (in iteration #1). Further, the removal of all Post-R1 units (iteration #4; Figure 12e) show additional change in the thicknesses of the units between the volcano and R1.

5 DISCUSSION

5.1 Volcanic **e**difices of the Miocene Mohakitino Volcanic Belt (MVB)

The tectonic setting of the study area (Figures 1a and 1c) and the characteristic features of the two dome-shaped structures within the syn- back-arc extension interval (Figures 4a, 5a-b, and 13a-b) suggest a volcanic origin. The onlapping of the younger stratigraphic sequences, suggesting its formation at the surface and its sub-flank-parallel reflections that downlap to a basal surface are similar to some interpretations of buried volcanoes in seismic data (eg. Infante-Paez and Marfurt, 2017; Infante-Paez, 2018; Jackson et al., 2019; Magee et al., 2013; Zhao et al., 2014). The size of the dome structures (~6.2 km diameter, measured from the abrupt increase of its slope; Figure 5a) is consistent with that of a modern volcano within the region (Mount Taranaki, ~6.5 km diameter; Figure 4a inset). Thus, we interpret that the dome-shaped features are volcanic seamounts, associated with the Middle to Late Miocene Mohakatino Volcanic Belt (MVB) of the Northern Taranaki Basin. The bright continuous reflector that defines the top of the volcanic edifice (R_0 reflector in Figure 5b) is associated with the large contrast in impedance response that characterize the interface between volcanic rocks and siliciclastic sediments (e.g., Infante-Paez and Marfurt, 2017).

We interpret the low-amplitude chaotic facies bounded by the domal reflector as the magmatic conduit of the edifice (Figure 5b). The aforementioned sub-vertical, steep reflectors that extend up through the central axis of the magma conduit are consistent with the velocity 'pull-up' (vpu) features observed in previous studies of volcanic bodies (e.g., Magee, 2013). These reflectors are useful for the estimation of seismic wave velocities through the volcanic bodies (Magee et al., 2013). It is also important to note that these features are not geologically related and can represent untrue structures in the time-migrated seismic data (Marfurt and Alves, 2015). Additionally, we deduce that the high-amplitude "saucer-shaped" reflectors beneath the R_0 reflector represents igneous sills, also consistent with the observations in previous studies (e.g., Infante-Paez and Marfurt, 2017; Magee, 2013). In our study area, the onlapping of stratigraphic reflectors on the R_0 surface (Figure 5b) suggests that the burial of the volcanic edifice is as a result of delivery of sediments from the New Zealand hinterland, onlapping onto the volcanic seamount.

5.2 Mechanisms of deformation of the post-MVB sedimentary sequences

Although we observe that in a few places, deep-seated faults propagate up into the clinoform packages (U1; Figures 2a, 9a, 9b), we primarily focus on the larger-scale influence of the buried MVB seamounts on the deformation of the clinoform packages. The deeper clinoforms and strata that overlie the buried seamounts show doming/folding patterns that systematically decrease in magnitude with shallowing depth from the top of the seamounts (Figure 5b and inset). This suggests that the vent of the magmatic conduit consists of a relatively more competent and denser rock, resulting in differential compaction of the overlying sediments (e.g., Reynolds et al., 2018).

Based on the observed systematic relationship between the buried seamounts and the associated overlying stratal doming, we interpret a differential compaction origin. At the time of deposition of the deeper clinoform packages, the weight of the overriding prograding sequences above the area of buried volcanoes would progressively load the underlying units, inducing a differential loading about the underlying rigid seamount. In response to the differential loading, the contrast in stiffness between the seamounts and the surrounding more-compressible sedimentary sequences would result in the differential compaction of the of the deeper units (e.g., Hansen and Cartwright, 2006), thus leading to the folding of the units. If the amplitudes of the folds are high enough (i.e. shallow burial of the mound peaks), the effect could propagate upwards and lead to the differential settling of the shallower unconsolidated sediments, thus influencing the local topography of the contemporary syn-depositional surface (Athy, 1930). In the following sections of our discussion below, we will demonstrate how the preexisting buried structures influenced the architecture of the overlying clinoform sequences by means of the mechanisms described above.

5.3 Regional evaluation of the younger clinoform sequences

Regional examination of the seismic profile provides the potential to understand how each unit varies structurally and internally with respect to the interpreted seismic facies, geometry and internal architectural elements. We have inferred that the high amplitude reflector (R2) that marks the boundary between Unit 1 and the onset of the next clinothem succession (Unit 2) abruptly truncates the interpreted canyon sized valleys defined by the V- and U-shaped continuous reflectors (Figures 4b-c). It is likely that this high amplitude response correlates to one of several observed condensed seismic intervals prominent within the GFF (Hansen and Kamp, 2002). Hansen and Kamp (2002, 2006) recognize these occurrences as a result of partial lithification of the horizons during relative sea level rise. There remains the potential to explore whether this is the cause for the distinct high amplitude response of surface R2 (Figure 4c). Although the prograding units U1 and U2 develop within the transition phase, we observe the collocation of a broad 'sag' geometry along both units in the southern domain of the study area, directly above a buried half-graben (Figures 4b-c). Additionally, we observe that thickest sections of an enclosed stratigraphic unit "MTD" within Unit U1 is collocated with underlying syn-extensional half grabens, separated by a thinner section that is collocated with an underlying syn-extensional horst block (Figure 8a). These observations suggest the influence of differential compaction of the syn- back-arc extension sequences caused by an imposed post-extension sediment loading along the axis of the buried horst-half graben structures. Thus, we interpret that buried syn-extension horst and graben structures may control the surface topography of evolving transition phase and post-extension depositional environments. This is consistent with observations in the Northern Graben, where the spatial distribution of clinoform height within the Pliocene-Recent strata show evidence of the control of the underlying normal fault structures (Salazar, 2015).

5.4 Controls of the Mohakitino Volcanic Complex on younger clinoform sequence boundaries

The known first-order controls on clinoform architecture and progradation are accommodation space and sediment supply (e.g., Emery and Myers, 1996). In our study area, we observe systematic relationships between the architecture of the clinoform packages and the underlying Mohakatino volcanic seamounts. First, we observe that overall, the N-S temporal variations (static) in the location of the 80% max. depth contour line along the two-way-travel time surfaces shows an initial landward migration (R1 to R2), followed by a consistently basinward migration (R2 to R4; Figures 7a-b). However, this initial landward migration is most evident in the central and southern domains of the study area. In the northern domain, two zones of inflection are present in the deeper units (U1 and U2), one proximal and the other distal of the volcanoes (Figures 6a and 7a), in which the largest maximum foreset angle is collocated with the proximal inflection point (Figure 8a). Also, the syn-depositional surface R2 in Figure 12d shows that the narrowest continental slope margin and steepened maximum foreset angle is collocated with the zone of significant flexural decompaction response to the east of the buried volcano. These observations suggest that the differential loading of the syn-extensional sequences about the buried volcano may have induced a temporal 'pinning' of the location (slowed basinward migration), width and steep geometry of the continental slope margin at the Time R2. The collocation of the slower migrating shelf in the northern domain with the compacted eastern flank of the buried Mohakatino volcanic seamounts (Figure 12d) suggests that the volcanic edifices may have temporally restricted the supply of sediment from the hinterlands into the basin of the northern domain. The absence of buried volcanoes in the central and southern domains may have allowed for the availability of more accommodation space further basinward, and no barrier to sediment supply. Furthermore, Progradational Style A (See Figure 7g) correlates with the highest recorded maximum foreset dips in the northern domain, where the buried seamounts are emplaced. This tells us that the volcanic seamounts influence the apparent progradational styles observed, such that the toe of the continental slope is not laterally consistent. Progradational Style B potentially correlates with the lower foreset dips in the central and southern domains, where the volcanic seamounts do not influence the lateral location of the toe-of-slope inflection point.

In addition, the along-trend geometry of the toe-of-slope inflection changes from a highly curvilinear/angular trend in the transition phase (R1 and R2), to a more rectilinear geometry within the post-extension interval (Unit-3 and shallower) (Figure 7a). This is also represented by the 80%max. depth contour line. We interpret that as sediment supply into the basin progressed, the geometry of the continental slope margin eventually becomes rectilinear as the central and southern domain shelf edge catches up with the slower migrating margin in the northern domain.

The break in slope of the depositional profile occurring between the topset and the clinoform (foreset) is the offlap break (Vail et al., 1991; Emery and Myers, 1996), and is previously defined as the shelf-edge in literature (See Figure 3). Overall, we find a prominence of stacked offlap breaks and over-steepened (7-10°) clinoform foreset slopes within the northern domain (Refer to Figure 13 a) transition phase clinoforms, and occurrence of gently dipping foreset slopes (<6°) in the southern domain (Refer to Figure 13c). Whereas, the post-extension clinoforms exhibit very low (<5°) and intermediate (5-7°) foreset slopes across the entire survey. Also, we observe that post-R2 loading of the area by the prograding sequences also induced more, although minor differential compaction of the deeper units (Figures 12b-c). This led to an additional flexure of the compacted units created the highly flexed geometry of the deeper units (units between the volcano and R1) seen in present-day (Figure 12a). Therefore, we further infer that the influence of the buried volcanoes on the post-extension sequences are not only syn-depositional, but also post-deposition of the clinoform packages. The observed temporal variations of the geometry of the post-extension sequences (units above the volcano) between the northern and southern domains of the study area suggest a systematic control of the buried volcanic structures in the northern domain.

We infer that the delivery of sediment along the oversteepened slopes within the deeper units (U1 up to Time R2) incised into the underlying stratigraphy forming canyon sized valleys (Figures 9a-b), that can be characterized as potential submarine canyons based on interpretations by Talling (1998). Their analyses characterize submarine canyon incisions to have depths greater than 70 m, coinciding with erosional processes, likely via turbidity currents. Additionally, Talling (1998) mention that pre-existing submarine canyons that are sub-aerially expose during sea level fall, tend to extend across the shelf-edge toward the continental coast. The seismic attribute stratal slices do not distinctly reveal extension of the canyon incision along the shelf edge (See Figure 9a). As the foreset angle becomes too steep, rapid deposition at the sudden decrease in slope occurs as turbidity currents will bypass the foreset - and with each succeeding flow of sediment packages and deposition on top of previously deposited material downslope, result in the backstepping of sediment (Refer to Figures 13d-h) onto the foreset, similar to observations defined by Gerber (2008). Such processes also indicate a period of high sediment supply. This may seem contradicting, since short-lived ovsersteeping of clinoform foresets have been linked to low rates of sediment supply into the basin (O'Grady et al., 2000; Shumaker et al., 2017) and/or the delivery of coarser grained sediment (Orton and Reading, 1993). O'Grady (2000) defines similar regional continental slope-geometries as "deep and steep" margins with dips ranging between 5-9.5°, consistent with high rates of canyon incision and mass wasting processes. The decrease in our measured foreset slope angles toward the southern domain, and following the position of the volcanic edifice, ranging between 4.3 - 6.5°, coincides with O'Grady's (2000) interpretation of relatively low sediment input of "steep and rough" margins (4.4 – 6.5° slope angles) and higher sediment supply of "sigmoid" margins (2.2 – 4.5) . This further stipulates the contribution of the placement of the volcanic seamount as a potential area of lateral confinement, influencing the geometry of the foreset slope and/or the migration of the progradational system.

Hansen and Kamp (2006) recognize that the northern "graben-bounding" faults have undergone displacement from the Pliocene into Pleistocene, controlling the patterns of deposition, regarding size and distribution in regional strata of the Giant Forests Formation. We suggest that the GFF, inferred from well summary reports, thickens toward the south where larger accommodation space is provided by southern extension of the graben, and its syn-depositional normal faults acting as the main depocentre for sediment deposition (Bierbrauer et al., 2008; Kamp and Furlong, 2006). The successions are structurally influenced by the paleo-topographic highs of the volcanic massifs closer to the continental shelf and deposition into the northern graben, while building and prograding northwestward/westward onto the Western Stable Platform. It is assumed that in the southernmost domain of the 3-D seismic, the perceived northwestern migration of the slope margin is consistent with the overall NW migration of the studied Giant Foresets formation, observed in previous studies (Salazar et al., 2016; Shumaker et al., 2017). On the contrary, the shelf-edge maintains a general westerly migration pattern as the Northern Graben depocentre opens up in the same direction but with axial movement likely limited by the basement high of the Western Stable Platform.

5.5 Associated architectural elements of the younger clinoforms

The stratigraphically-enclosed body ("MTD" in Figure 8c) consisting of a mostly chaotic seismic character of high discontinuous variance zones, with globular low variance values is identified as coherent displaced rock consistent with mass transport deposits (MTDs), a common component of deep-water settings. The occurrence of the MTD (Figures 8a-c) above reflector R1 (within Unit 1) during Mid Pliocene is imaged clearly by the variance attribute as a result of the significant variations and structural discontinuity in its seismic trace patterns. They are consistent with great degrees of slope failure triggered by regression during rapid sea level fall, high sedimentation rates, seismicity and gas hydrate destabilization (Moscardelli and Wood, 2008; Rusconi, 2017). Rusconi (2017) studied MTD's in the Taranaki Basin within the Pliocene to Pleistocene interval, linking their occurrence to oversteepening of the slopes due to high sediment influx to the shelf edge and seismicity related to back arc extension. It is therefore possible that this erosional feature located below surface R2, and which truncates parallel amplitude reflectors (See Figure 8a) on both sides in the central region of the volume, likely occurred during the basinward outbuilding of Unit 1, since it coincides with the back arc extension tectonics. Internal clinoform architectural elements are more prominent within Unit 2 as more channelized geometries are also highlighted along the curvature attribute surfaces (Figures 10a and 10c). Here, we interpret a slump feature, which (Refer to Figure 10a and 10b) associated with periods of falling sea level, in which unstable slope conditions persist due to over-pressuring (Postma, 1984) during sediment accumulation, and a depositional fan lobe toward the south, coherent with mud/sand rich systems distinctly encapsulated by the high positive RMS amplitude response. We've linked, via interpretations by Bierbrauer (2008), the top of Unit 2 to the end of a falling stage systems tract, before the initiation of a high-stand systems tract. The basin was perhaps experiencing increasing sediment bypass forming the aforementioned principal elements of deep-marine clastic systems. The system then experienced an increase in sediment supply with steady rise in sea level, as the sequence boundary at the base of our interpreted Unit 3 (top Unit 2), coincides with the high-stand systems tract interpreted by Bierbrauer (2008). The timing of this increasing sediment supply, and overall decreasing maximum foreset angles, can be further be supported by the increase in uplift of the Southern Alps ~3 Myr ago in Late Pliocene, supplying sediment across the Taranaki Basin (Tippet and Kamp, 1995; Salazar et al., 2015)

Unit 3 consists of shallower foreset and topset gradients as further supported by the mapped negative curvature stratal slices (Figure 11), indicating the overall transition to a sediment driven arrangement as the progradation system migrated toward and onto the Western Stable Platform (Shumaker et al., 2017). The more recent sequence of this unit is characterized by a dense network of linear channels that feed into the basin (Figure 11). These regularly spaced channels have been defined as submarine gullies, originating at the shelf-edge (Shumaker et al., 2016). The shelf edge has migrated significantly basinward (S2 and S8), and the network of the gullies are predominant throughout the northern to southernmost domains of the horizon surface. The RMS amplitude also reveal high positive responses within the confines of the northern and southern highlighted gullies (Figure 11b), again discriminating the lithological variations across the surface. The Giant Foresets Formation is a claystone to siltstone dominated succession comprising of intervals of argillaceous sandstone (O'Leary et al., 2010) and is generally a thick coarsening upward sequence commencing in late Miocene further south near the Awatea-1 well (Hansen and Kamp, 2006; O'Leary et al., 2010) and commencing in early Pliocene in our area of study. With the interpretations of Bierbrauer (2008), and our observations, we assume that this coarsening upward sequence explains the increase in channelization or gully formation coinciding with a high energy transport environment and increased erosion and deposition as the gullies partially incise into the paleo-seafloor.

5.6 Implications for the influence of preexisting structures on the architecture of deep-water progradational sequences

Few studies have highlighted the potential influence of buried structural features on subsequent sedimentary sequences (Hardage et al., 1996; Tsikalas, et al., 1998; Anka et al., 2009; Alves, 2010; Johnston et al., 2010). Our observations in the Northern Taranaki Basin expand on these previous works by demonstrating that buried, discrete, massive, relatively more- or less-stiff structures may significantly modulate the geometry of syn-depositional surfaces and the post-depositional architecture of deep-water progradational sequences. These features may include, but are not limited to paleovolcanoes, mass transport deposits, impact craters, carbonate mounds & karst features, horst-graben structures etc.

Furthermore, our findings highlight important controls on post-extensional sedimentation patterns in magmatic continental margins that contrast those of non-magmatic margins. For example, in the case of rifted margins, the global distribution of magmatic and non-magmatic rifted margins (e.g., Geoffroy, 2005; Leroy at al., 2008) suggests that there is a significant percentage of magmatic rifted margins. Magmatic rifted margins account for approximately 80% of the total distribution, with 20% being the known non-magmatic or magma-poor regions. The Northern Taranaki Basin is located within a back-arc setting of a previously rifted margin, and therefore is not a true passive margin in its present form. However, the structures potentially present features that may be observable in rifted margins that have accommodated magmatic deformation. In the central domain of our study area where buried volcanoes are absent, we observe the differential compaction of the syn- and post-extension sedimentary packages influenced by buried horst-graben structures. This indicates that the buried syn-extensional horst-graben structures may partially control the topography of the succeeding depositional environment (e.g., Figures 8a, 4c, and 14). The modulation of the topography would have a spatial wavelength that is consistent with the extents and geometry of the buried structure (e.g., Figure 8a). We envision that such controls on post-extension sedimentary architecture may be observable in both magmatic and non-magmatic rifted regions. However, the presence of paleovolcanoes in the deeper strata of rifted margins having magmatic deformation constitute relatively 'smaller' (shorter-wavelength) structures that are super-imposed on the longer-wavelength syn-extension horst-graben structures (Figure 14). We infer that the superposition of buried syn-extension volcanoes on their contemporary longer-wavelength horst-graben structures in magmatic rifted margins represents an important distinction on the controls of post-extension progradational sedimentation patterns that contrasts those of rifted margins that have not accommodated magmatic deformation (Figure 14). Overall, in relation to both divergent and convergent continental margins, we have shown that the architecture and sedimentation patterns reveal a relationship between buried volcanic structures and succeeding post-magmatism progradational stratigraphic successions, such that we observe high maximum foreset angles; relative temporal pinning of the continental slope; and a transition from accommodated erosional features such as submarine canyon incision, mass transport deposits, and slumps to less erosional and more depositional channelized features (submarine gullies) as the system progrades.

CONCLUSIONS

We investigated the controls of buried syn-back-arc extension seamounts on the post-extension sedimentation patterns within the Northern Taranaki Basin. Our results reveal that overall, the N-S trend of continental slope margin changes from a highly curvilinear geometry in the deeper post-extension sequences (transition phase), into a rectilinear trend within the shallower post-extension sequences. In the northern domain of the study area where the buried seamounts dominate, the overlying clinoform packages and sequence boundaries show folding that systematically decrease in magnitude with shallowing depth from the top of the underlying seamounts. In this same part of the area, we observe aggradational type seismic facies, clinoform oversteepening and backstepping, high foreset slope angles, and relatively slower continental slope margin basinward migration (temporally 'pinned') in the post- extension sequences above the buried volcanoes.

Whereas, in the southern domain, where buried volcanoes are absent, we observe more progradational type seismic facies, very low foreset slope angles, and landward-to-basinward ('unpinned') migration of the continental slope margin. Additionally, in the northern domain, we observe wide, closely spaced channel incision into over-steepened slope dominate the post-extension sequence in the northern domain. Whereas, narrower, straighter channels dominate the southern domain. These findings suggest that buried syn-extension volcanic massifs can significantly influence the architecture of the succeeding progradational sedimentary successions. Our study provides insight into the controls of preexisting buried discrete, massive, relatively more- or less-stiff structures on the development of the onset of deep-water progradational sequences, such that we observe high maximum foreset angles; relative temporal pinning of the continental slope; and a transition from accommodated erosional features such as submarine canyon incision, mass transport deposits, and slumps to less erosional and more depositional channelized features (submarine gullies) as the system progrades. Furthermore, we suggest that our findings in this work present a distinction in the controls on sedimentation patterns between magmatic and non-magmatic continental margins. that we

ACKOWLEDGEMENTS

We would sincerely like to thank New Zealand Petroleum & Minerals and Origin Energy New Zealand Pty Ltd for providing the Nimitz 3D data set. Additionally, we express our greatest appreciation to Petrel E&P software from Schlumberger for providing the University of

Oklahoma with the academic licenses for conducting this project as well as the AASPI (Attribute-Assisted Seismic Processing and Interpretation) consortium here at the University of Oklahoma. We thank CGG for providing the Hampson Russell academic license used for this study and Badley's Geoscience Ltd for providing the FlexDecomp software. We thank Abidin Caf for assisting within the seismic-to-well tie. We also thank the Editor Craig Magee, reviewer Mac Beggs and the second, anonymous, reviewer.

Data Availability Statement: The data that support the findings of this study are publicly available on the New Zealand Petroleum and Minerals website www.nzpam.govt.nz, and can be acquired without any privacy or ethical restrictions.

Funding Statement: The first author of this manuscript, Roberto Clairmont, is a graduate student, whom was funded to perform this research with research funds delegated by Dr. Heather Bedle. No external funding was provided for this study.

Declaration of interests:

☒ The authors declare that they have no known competing financial interests or personal relationships that could have appeared to influence the work reported in this paper.

Permission to reproduce material from other sources:

We have not reproduced any material from other sources.

REFERENCES

Allen, P., and Allen, J. R. (2006). Basin analysis. Principles and applications 2nd edn, Blackwell Scientific Publications. Oxford, p. 549p.

Alves, T. M. (2010). 3D Seismic examples of differential compaction in mass-transport deposits and their effect on post-failure strata. Marine Geology, 271(3–4), 212–224. https://doi.org/10.1016/j.margeo.2010.02.014

Amonpantang, P., Bedle, H., & Wu, J. (2019). Multiattribute analysis for channel element discrimination in the Taranaki Basin, offshore New Zealand. Interpretation, 7(2), SC45–SC61. https://doi.org/10.1190/INT-2018-0174.1

Anell, I., & Midtkandal, I. (2017). The quantifiable clinothem—Types, shapes and geometric relationships in the Plio-Pleistocene Giant Foresets Formation, Taranaki Basin, New Zealand. Basin Research, 29, 277–297. https://doi.org/10.1111/bre.12149

Anka, Z., Séranne, M., Lopez, M., Scheck-Wenderoth, M., & Savoye, B. (2009). The long-term evolution of the Congo deep-sea fan: A basin-wide view of the interaction between a giant submarine fan and a mature passive margin (ZaiAngo project). Tectonophysics, 470(1–2), 42–56. https://doi.org/10.1016/j.tecto.2008.04.009

Armstrong, P. A., Allis, R. G., Funnell, R. H., and Chapman, D. S. (1998). Late Neogene exhumation patterns in Taranaki Basin (New Zealand): Evidence from offset porosity-depth trends: Journal of Geophysical Research: Solid Earth, v. 103, no. B12, p. 30269-30282.

Athy, L.F. (1930). Density, porosity, and compaction of sedimentary rocks. Aapg Bulletin, 14(1), pp.1-24.

Berton, F., Vesely, F. F., & Universidade Federal do Paraná, Brazil. (2016). Seismic expression of depositional elements associated with a strongly progradational shelf margin: Northern Santos Basin, southeastern Brazil. Brazilian Journal of Geology, 46(4), 585–603. https://doi.org/10.1590/2317-4889201620160031

Bierbrauer, K., Herdy, T.J., Rek, A. & Mills K.L. (2008). Offshore Northland Basin - Frontier exploration north of the established Taranaki Hydrocarbon Province. Origin Energy Limited, 18.

Bischoff, A. P., Nicol, A., & Beggs, M. (2017). Stratigraphy of architectural elements in a buried volcanic system and implications for hydrocarbon exploration. Interpretation, 5(3), SK141–SK159. https://doi.org/10.1190/INT-2016-0201.1

Bridgwater, D., Sutton, J. and Watterson, J. (1974). Crustal downfolding associated with igneous activity. Tectonophysics, 21(1-2), pp.57-77.

Chen, Q., & Sidney, S. (1997). Seismic attribute technology for reservoir forecasting and monitoring. The Leading Edge, 16(5), 445–448. https://doi.org/10.1190/1.1437657

Chopra, S., & Marfurt, K. J. (2008). Emerging and future trends in seismic attributes. The Leading Edge, 27(3), 298–318. https://doi.org/10.1190/1.2896620

Chopra, S., Marfurt, K. (2013) Structural curvature versus amplitude curvature. The Leading Edge. Pgs 178-184.

Emery, D. and Myers, K.J. (1996). Sequence Stratigraphy. Blackwell Science, Oxford, 297. http://dx.doi.org/10.1002/9781444313710

Feuillet, N., Manighetti, I., Tapponnier, P. and Jacques, E. (2002). Arc parallel extension and localization of volcanic complexes in Guadeloupe, Lesser Antilles. Journal of Geophysical Research: Solid Earth, 107(B12), pp.ETG-3.

Gerber, T. P., Pratson, L. F., Wolinsky, M. A., Steel, R., Mohr, J., Swenson, J. B., Paola, C. (2008). Clinoform Progradation by Turbisity Currents: Modeling and Experiments. Journal of Sedimentary Research; 78 (3), 220-238. https://doi.org/10.2110/jsr.2008.023

Geoffroy, L. (2005). Volcanic passive margins. Comptes Rendus Geoscience, 337(16), 1395–1408. https://doi.org/10.1016/j.crte.2005.10.006

Giba, M., Nicol, A., & Walsh, J. J. (2010). Evolution of faulting and volcanism in a back-arc basin and its implications for subduction processes: Taranaki Basin Evolution. Tectonics, 29(4), n/a-n/a. https://doi.org/10.1029/2009TC002634

Giba, M., Walsh, J. J., Nicol, A., Mouslopoulou, V., & Seebeck, H. (2013). Investigation of the spatio-temporal relationship between normal faulting and arc volcanism on million-year time scales. Journal of the Geological Society, 170(6), 951–962. https://doi.org/10.1144/jgs2012-121

Gomes, M. P., Vital, H., Bezerra, F. H. R., de Castro, D. L., & Macedo, J. W. de P. (2014). The interplay between structural inheritance and morphology in the Equatorial Continental Shelf of Brazil. Marine Geology, 355, 150–161. https://doi.org/10.1016/j.margeo.2014.06.002

Gomis-Cartesio, L. E., Poyatos-Moré, M., Hodgson, D. M., & Flint, S. S. (2018). Shelf-margin clinothem progradation, degradation and readjustment: Tanqua depocentre, Karoo Basin (South Africa). Sedimentology, 65(3), 809–841. https://doi.org/10.1111/sed.12406

Gong, C., Wang, Y., Zhu, W., Li, W., Xu, Q., & Zhang, J. (2011). The Central Submarine Canyon in the Qiongdongnan Basin, northwestern South China Sea: Architecture, sequence stratigraphy, and depositional processes. Marine and Petroleum Geology, 28(9), 1690–1702. https://doi.org/10.1016/j.marpetgeo.2011.06.005

Hansen, R. J., & Kamp, P. J. (2002). Evolution of the Giant Foresets Formation, northern Taranaki Basin, New Zealand. 18.

Hansen, R. J., & Kamp, P. J. J. (2004a). Late Miocene to early Pliocene stratigraphic record in northern Taranaki Basin: Condensed sedimentation ahead of Northern Graben extension and progradation of the modern continental margin. New Zealand Journal of Geology and Geophysics, 47(4), 645–662. https://doi.org/10.1080/00288306.2004.9515081

Hansen, R., & Kamp, P. (2004b). Rapid progradation of the Pliocene-Pleistocene continental margin, northern Taranaki Basin, New Zealand, and implications. 10.

Hansen, D.M. and Cartwright, J.A. (2006). The three-dimensional geometry and growth of forced folds above saucer-shaped igneous sills. Journal of Structural Geology, 28(8), pp.1520-1535.

Hansen, R. J., & Kamp, P. J. J. (2006). Sequence stratigraphy and architectural elements of the Giant Foresets Formation, northern Taranaki Basin, New Zealand. 13.

Hardage, B. A., Carr, D. L., Lancaster, D. E., Simmons, J. L., Elphick, R. Y., Pendleton, V. M., & Johns, R. A. (1996). 3-D seismic evidence of the effects of carbonate karst collapse on overlying clastic stratigraphy and reservoir compartmentalization. GEOPHYSICS, 61(5), 1336–1350. https://doi.org/10.1190/1.1444057

Heezen, B. C., Hollister, C. D., & Ruddiman, W. F. (1966). Shaping of the Continental Rise by Deep Geostrophic Contour Currents. Science, 152(3721), 502–508. https://doi.org/10.1126/science.152.3721.502

Herzer, R. H. (1995). Seismic stratigraphy of a buried volcanic arc, Northland, New Zealand and implications for Neogene subduction. Marine and Petroleum Geology, 12, 511–531.

Holford, S., Schofield, N., MacDonald, J., Duddy, I. and Green, P. (2012). Seismic analysis of igneous systems in sedimentary basins and their impacts on hydrocarbon prospectivity: Examples from the southern Australian margin. The APPEA Journal, 52(1), pp.229-252.

Hood, S. D., Nelson, C. S., & Kamp, P. J. J. (2003). Lithostratigraphy and depositional episodes of the Oligocene carbonate-rich Tikorangi Formation, Taranaki Basin, New Zealand. New Zealand Journal of Geology and Geophysics, 46(3), 363–386. https://doi.org/10.1080/00288306.2003.9515015

Infante-Paez, L., & Marfurt, K. J. (2017). Seismic expression and geomorphology of igneous bodies: A Taranaki Basin, New Zealand, case study. Interpretation, 5, SK121-SK140.

Infante-Paez, L. (2018). Seismic expression of igneous bodies in sedimentary basins and their impact on hydrocarbon exploration: Examples from a compressive tectonic setting, Taranaki Basin, New Zealand. PhD. Dissertation, University of Oklahoma.

Jackson, C.A., Schofield, N. and Golenkov, B. (2013). Geometry and controls on the development of igneous sill–related forced folds: A 2-D seismic reflection case study from offshore southern Australia. Bulletin, 125(11-12), pp.1874-1890.

Jackson, C.A., Magee, C. and Hunt-Stewart, E.R. (2019). Cenozoic contourites in the eastern Great Australian Bight, offshore southern Australia: implications for the onset of the Leeuwin Current. Journal of Sedimentary Research, 89(3), pp.199-206.

Johnston, S., Strachan, L., Cassidy, J. (n.d.). Late Pliocene to Recent Seismic Stratigraphy of the Northland Basin, New Zealand, #50327 (2010). 33.

Kamp, P.J.J. (1984). Neogene and Quaternary extent and geometry of the subducted Pacific Plate beneath North Island, New Zealand: Implications for Kaikoura tectonics. Tectonophysics, 108, 241–266.

Kamp, P. J. J., & Furlong, K. P. (2006). Neogene Plate Tectonic Reconstructions and Geodynamics of North Island Sedimentary Basins: Implications for the Petroleum Systems. 14.

King, P.R. and Thrasher, G.P. (1996) Cretaceous-Cenozoic geology and petroleum systems of the Taranaki Basin, New Zealand. Institute of Geological and Nuclear Sciences monograph 13. 243 p. 6 enclosures. Institute of Geological and Nuclear Scienses Ltd., Lower Hutt.

King, P. R., 2000, Tectonic reconstructions of New Zealand: 40 Ma to the present: New Zealand Journal of Geology and Geophysics, 43, 611–638.

Kolawole, F., Simpson-Turko M., & Carpenter, B. M. (2020). Basement-Controlled Deformation of Sedimentary Sequences, Anadarko Shelf, Oklahoma. Basin Research.

Leroy, M., Gueydan, F., & Dauteuil, O. (2008). Uplift and strength evolution of passive margins inferred from 2-D conductive modelling. Geophysical Journal International, 172(1), 464–476. https://doi.org/10.1111/j.1365-246X.2007.03566.x

Lodwick, George, Rupert, Maguire (2019). What controls the reservoir quality of andesitic arc derived volcano clastic sandstone reservoirs: An example from the Mohakatino Formation, Taranaki Basin, New Zealand, Durham theses, Durham University. Available at Durham E-Theses Online:http://etheses.dur.ac.uk/13239/

Magee, C., Hunt-Stewart, E., & Jackson, C. A.-L. (2013). Volcano growth mechanisms and the role of sub-volcanic intrusions: Insights from 2D seismic reflection data. Earth and Planetary Science Letters, 373, 41–53. https://doi.org/10.1016/j.epsl.2013.04.041

Magee, C., Muirhead, J.D., Karvelas, A., Holford, S.P., Jackson, C.A., Bastow, I.D., Schofield, N., Stevenson, C.T., McLean, C., McCarthy, W. and Shtukert, O. (2016). Lateral magma flow in mafic sill complexes. Geosphere, 12(3), pp.809-841.

Magee, C., Stevenson, C. T. E., Ebmeier, S. K., Keir, D., Hammond, J. O. S., Gottsmann, J. H., Whaler, K. A., Schofield, N., Jackson, C. A.-L., Petronis, M. S., O'Driscoll, B., Morgan, J., Cruden, A., Vollgger, S. A., Dering, G., Micklethwaite, S., & Jackson, M. D. (2018). Magma Plumbing Systems: A Geophysical Perspective. Journal of Petrology, 59(6), 1217–1251. https://doi.org/10.1093/petrology/egy064

Marfurt, K. J., & Alves, T. M. (2015). Pitfalls and limitations in seismic attribute interpretation of tectonic features. Interpretation, 3(1), SB5–SB15. https://doi.org/10.1190/INT-2014-0122.1

Mitchum, R. M. (1977). Seismic Stratigraphy and Global Changes of Sea Level, Part 11: Glossary of Terms used in Seismic Stratigraphy. 8.

Mortimer, E.J., Paton, D.A., Scholz, C.A. and Strecker, M.R. (2016). Implications of structural inheritance in oblique rift zones for basin compartmentalization: Nkhata Basin, Malawi Rift (EARS). Marine and Petroleum Geology, 72, pp.110-121.

Moscardelli, L., & Wood, L. (2008). New classification system for mass transport complexes in offshore Trinidad. Basin Research, 20(1), 73–98. https://doi.org/10.1111/j.1365-2117.2007.00340.x

Muirhead, J.D., Airoldi, G., Rowland, J.V. and White, J.D. (2012). Interconnected sills and inclined sheet intrusions control shallow magma transport in the Ferrar large igneous province, Antarctica. Bulletin, 124(1-2), pp.162-180.

Murdmaa, I. O., Levchenko, O. V., & Marinova, J. G. (2012). Quaternary seismic facies of the atlantic continental rise. Lithology and Mineral Resources, 47(5), 379–400. https://doi.org/10.1134/S0024490212050069

Nicol, A., Mazengarb, C., Chanier, F., Rait, G., Uruski, C., & Wallace, L. (2007). Tectonic evolution of the active Hikurangi subduction margin, New Zealand, since the Oligocene: Hikurangi Subduction Margin Tectonics. Tectonics, 26(4), n/a-n/a. https://doi.org/10.1029/2006TC002090

O'Grady, D. B., Syvitski, J. P. M., Pratson, L. F., & Sarg, J. F. (2000). Categorizing the morphologic variability of siliciclastic passive continental margins. 4.

O'Grady, D. B., & Syvitski, J. P. M. (2002). Large-scale morphology of Arctic continental slopes: The influence of sediment delivery on slope form. Geological Society, London, Special Publications, 203(1), 11–31. https://doi.org/10.1144/GSL.SP.2002.203.01.02

O'Leary, R. Luft, F. and Mogg, W. Origin Energy New Zealand Pty Ltd (2010). Ministry of Economic Development New Zealand Unpublished Petroleum Report 4299. 401

Orton, G. J., & Reading, H. G. (1993). Variability of deltaic processes in terms of sediment supply, with particular emphasis on grain size. Sedimentology, 40(3), 475–512. https://doi.org/10.1111/j.1365-3091.1993.tb01347.x

Palmer, J. (1985). Pre-Miocene lithostratigraphy of Taranaki Basin, New Zealand. New Zealand journal of geology and geophysics, 28, 197-216.

Patruno, S., & Helland-Hansen, W. (2018). Clinoforms and clinoform systems: Review and dynamic classification scheme for shorelines, subaqueous deltas, shelf edges and continental margins. Earth-Science Reviews, 185, 202–233. https://doi.org/10.1016/j.earscirev.2018.05.016

Postma, G. (1984). Slumps and their deposits in fan delta front and slope. 4

Puga-Bernabéu, Á., Vonk, A. J., Nelson, C. S., & Kamp, P. J. J. (2009). Mangarara Formation: Exhumed remnants of a middle Miocene, temperate carbonate, submarine channel-fan system on the eastern margin of Taranaki Basin, New Zealand. New Zealand Journal of Geology and Geophysics, 52(2), 73–93. https://doi.org/10.1080/00288300909509880

Randen, T., Pedersen, S. I., & Sønneland, L. (2001). Automatic extraction of fault surfaces from three-dimensional seismic data. SEG Technical Program Expanded Abstracts 2001, 551–554. https://doi.org/10.1190/1.1816675

Reynolds, P., Schofield, N., Brown, R. J., & Holford, S. P. (2018). The architecture of submarine monogenetic volcanoes—Insights from 3D seismic data. Basin Research, 30, 437–451. https://doi.org/10.1111/bre.12230

Rusconi, F. J. (n.d.). 3D Seismic Interpretation of a Plio-Pleistocene Mass Transport Deposit in the Deepwater Taranaki Basin of New Zealand. (2017). 62.

Salazar, M., Moscardelli, L., & Wood, L. (2016). Utilising clinoform architecture to understand the drivers of basin margin evolution: A case study in the Taranaki Basin, New Zealand. Basin Research, 28(6), 840–865. https://doi.org/10.1111/bre.12138

Sclater, J. G., and Christie, P. A. (1980). Continental stretching: An explanation of the post-mid-Cretaceous subsidence of the central North Sea basin: Journal of Geophysical Research: Solid Earth, v. 85, no. B7, p. 3711-3739.

Seebeck, H.C. (2012). Normal Faulting, Volcanic and Fluid Flow, Hikurangi Subduction Plate Boundary, New Zealand. PhD. Dissertation, University of Canterbury. 113-151

Seebeck, H., Nicol, A., Villamor, P., Ristau, J., & Pettinga, J. (2014). Structure and kinematics of the Taupo Rift, New Zealand: Taupo Rift. Tectonics, 33(6), 1178–1199. https://doi.org/10.1002/2014TC003569

Shumaker, L. E., Jobe, Z. R., & Graham, S. A. (2017). Evolution of submarine gullies on a prograding slope: Insights from 3D seismic reflection data. Marine Geology, 393, 35–46. https://doi.org/10.1016/j.margeo.2016.06.006

Slingerland, R., Driscoll, N. W., Milliman, J. D., Miller, S. R., & Johnstone, E. A. (2008). Anatomy and growth of a Holocene clinothem in the Gulf of Papua. Journal of Geophysical Research, 113(F1), F01S13. https://doi.org/10.1029/2006JF000628

Stagpoole, V., & Funnell, R. (2001). Arc magmatism and hydrocarbon generation in the northern Taranaki Basin, New Zealand. Petroleum Geoscience, 7(3), 255–267. https://doi.org/10.1144/petgeo.7.3.255

Stagpoole, V., & Nicol, A. (2008). Regional structure and kinematic history of a large subduction back thrust: Taranaki Fault, New Zealand. Journal of Geophysical Research, 113(B1), B01403. https://doi.org/10.1029/2007JB005170

Steel R.J & Olsen T. (2002). Clinoforms, clinoform trajectories and deepwater sands. In: Armentrout J.M. & Rosoen N.C. (Eds.). Sequence stratigraphic models fpr exploration and production: evolving models and appkication histories, GCS-SEPM Special Publication, 22: 367-381.

Talling, P. J. (1998). How and where do incised valleys form if sea level remains above the shelf edge? 4.

Tippett, J. M., & Kamp, P. J. J. (1995). Geomorphic evolution of the Southern Alps, New Zealand. Earth Surface Processes and Landforms, 20(2), 177–192. https://doi.org/10.1002/esp.3290200207

Tsikalas, F., Gudlaugsson, S. T., & Faleide, J. I. (1998). The anatomy of a buried complex impact structure: The Mjølnir Structure, Barents Sea. Journal of Geophysical Research: Solid Earth, 103(B12), 30469–30483. https://doi.org/10.1029/97JB03389

Unkaracalar, E. E. 3D seismic imaging of submarine stratovolcanic and salt structures beneath the Taranaki Basin, New Zealand and the Gulf of Mexico (2018). Masters Theses. 7787. http://scholarsmine.mst.edu/masters_theses/7787

Uruski, C., & Baillie, P. (2004). Mesozoic evolution of the Greater Taranaki Basin and implications for petroleum prospectivity. The Appea Journal, 44(1), 385. https://doi.org/10.1071/AJ03014

Vail, PR. (1987). Seismic stratigraphy interpretation using sequence stratigraphy. Part I: Seismic stratigraphy interpretation procedure. In Atlas of Seismic Stratigraphy, ed. AW Bally, pp. 1-10. Am. Assoc. Petrol. Geol. Stud. Geol. No. 27, Vol. 1. 125 pp

Vail, P.R., Audemart, F., Bowman, S.A., Eisner, P.N, Perez-Cruz, G. (1991). The stratigraphic signatures of tectonics, eustasy and sedimentation – an overview. In: cyclic Stratigraphy (ed. By G.Einsele, W. Ricken & Seilacher). Springer-Verlag, New York, pp. 617-659.

Zhao, F., Wu, S., Sun, Q., Huuse, M., Li, W., & Wang, Z. (2014). Submarine volcanic mounds in the Pearl River Mouth Basin, northern South China Sea. Marine Geology, 355, 162–172. https://doi.org/10.1016/j.margeo.2014.05.018

FIGURES

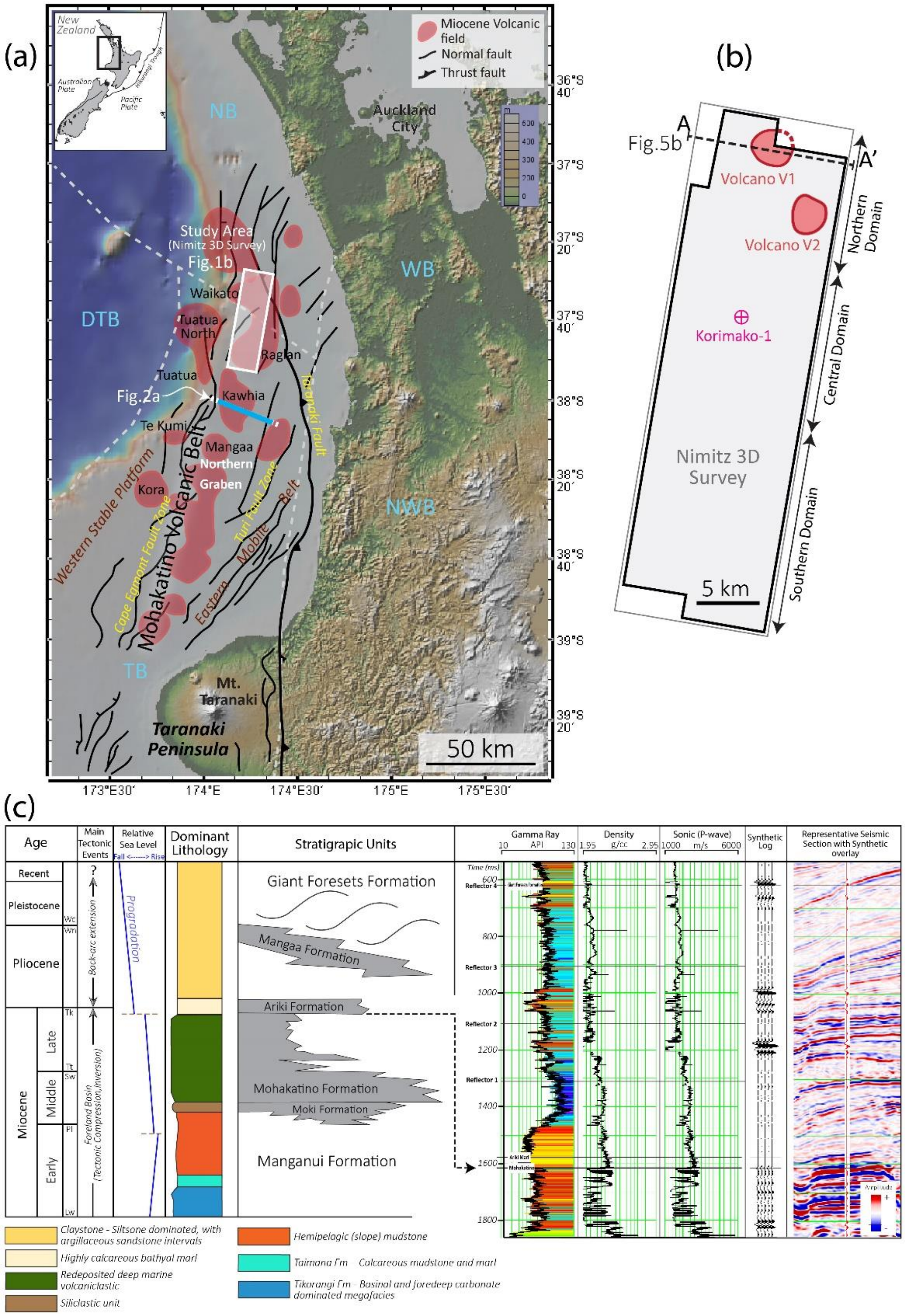
(a)
New Zealand
Miocene Volcanic field
Normal fault
Thrust fault
NB
Auckland City
DTB
WB
NWB
TB
Study Area
(Nimitz 3D Survey)
Fig.1b
Waikato
Tuatua North
Raglan
Tuatua
Fig.2a
Kawhia
Te Kumi
Mangaa
Northern Graben
Kora
Western Stable Platform
Cape Egmont Fault Zone
Mohakatino Volcanic Belt
Turi Fault Zone
Eastern Mobile Belt
Taranaki Fault
Mt. Taranaki
Taranaki Peninsula
50 km
173°E30′
174°E
174°E30′
175°E
175°E30′
(b)
Fig.5b
A
A′
Volcano V1
Volcano V2
Korimako-1
Northern Domain
Central Domain
Southern Domain
Nimitz 3D Survey
5 km
(c)
Age
Main Tectonic Events
Relative Sea Level
Dominant Lithology
Stratigrapic Units
Gamma Ray
Density
Sonic (P-wave)
Synthetic Log
Representative Seismic Section with Synthetic overlay
Recent
Pleistocene
Pliocene
Miocene
Late
Middle
Early
Back-arc extension
Foreland Basin (Tectonic Compression, Inversion)
Progradation
Giant Foresets Formation
Mangaa Formation
Ariki Formation
Mohakatino Formation
Moki Formation
Manganui Formation
Claystone - Siltsone dominated, with argillaceous sandstone intervals
Highly calcareous bathyal marl
Redeposited deep marine volcaniclastic
Siliclastic unit
Hemipelagic (slope) mudstone
Taimana Fm Calcareous mudstone and marl
Tikorangi Fm Basinal and foredeep carbonate dominated megafacies

Figure 1. Location and the geologic setting of the study area. (a) Topographic map of northern New Zealand showing the Taranaki and Northland Basins, large faults, and the Miocene volcanic fields of the Mohakatino Volcanic Belt (modified after Stagpoole & Funnell, 2001 and Johnston et al., 2010). The location of the primary study area (Nimitz 3-D Seismic Survey) is shown in the white rectangle, together with a 2D transect line used to show the extent of interpreted geologic features, discussed throughout this expert. (b) Map of the Nimitz 3-D seismic survey and location of the Korimako-1 well. (c) Generalized stratigraphic column of the upper fill of the Taranaki Basin (after Unkaracalar, 2018 and King and Thrasher, 1996), and generated wireline logs and synthetic model of the Korimako-1 well. The following stage abbreviations reflect the local geology of the area; Wc-Castlecliffian, Wn-Nukumaruan, Wo-Opoitian, Tk-Kapitean, Tt-Tongaporutuan, Sw-Waiauan, Sc-Clifdenian, Pl-Altonian, Lw-Waitakian). Predominant Formation lithologies are classified based on observations by Hood (2003), Puga-Bernabéu (2009) and O'Leary (2010). DTB – Deepwater Taranaki Basin, NB – Northland Basin, NWB - North Wanganui Basin, WB – Waikato Basin, TB – Taranaki Basin.

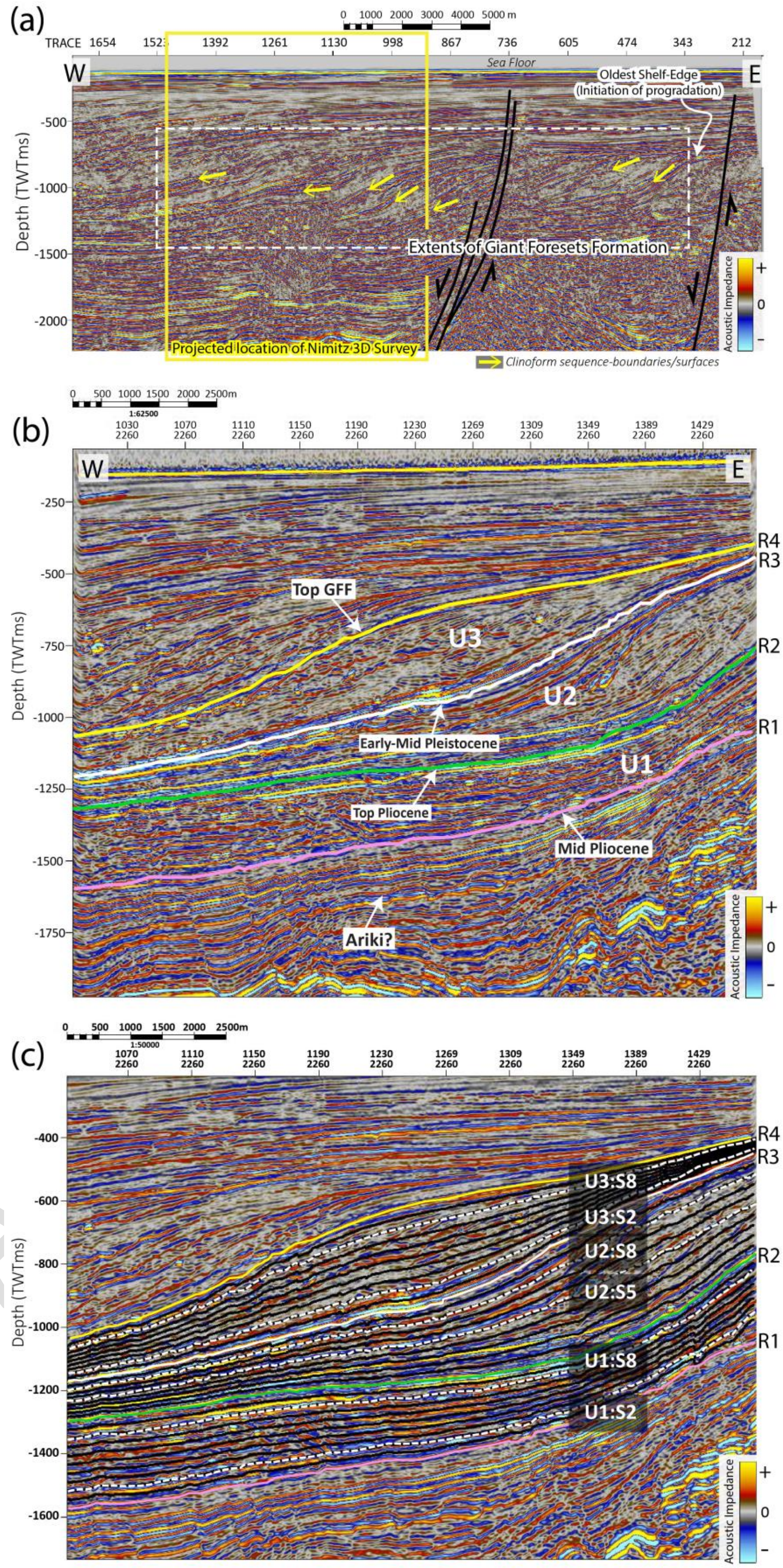
(a)
0 1000 2000 3000 4000 5000 m
TRACE 1654 1523 1392 1261 1130 998 867 736 605 474 343 212
Sea Floor
W
E
Oldest Shelf-Edge
(Initiation of progradation)
Depth (TWTms)
-500
-1000
-1500
-2000
Extents of Giant Foresets Formation
Projected location of Nimitz 3D Survey
Clinoform sequence-boundaries/surfaces
Acoustic Impedance
+
0
-
(b)
0 500 1000 1500 2000 2500m
1:62500
W
E
Depth (TWTms)
-250
-500
-750
-1000
-1250
-1500
-1750
R4
R3
R2
R1
Top GFF
U3
U2
U1
Early-Mid Pleistocene
Top Pliocene
Mid Pliocene
Ariki?
Acoustic Impedance
(c)
0 500 1000 1500 2000 2500m
1:50000
Depth (TWTms)
-400
-600
-800
-1000
-1200
-1400
-1600
R4
R3
R2
R1
U3:S8
U3:S2
U2:S8
U2:S5
U1:S8
U1:S2
Acoustic Impedance

Figure 2. Post back-arc extension progradational features. (a) Cross section (CNL95B-38) showing the 2D transect (See Figure 1a) with the oldest interpreted shelf-edge and the location of the onset of clinoform progradation. The box encloses the lateral extent of the known Giant Foresets Formation within the Taranaki Basin. (b) Cross-section showing the mapped key horizons (four reflectors - R1, R2, R3, R4) of the Nimitz Survey which bound Units 1 – 3 and potential formation tops, supported by both well-ties and literature (O'Leary et al., 2010) (b) A zoom-in of the mid-section of Figure 2b showing stratal slices generated within the units and the dashed, labeled slices used for surface horizon interpretation. See Figure S1 for the a larger uninterpreted version of the seismic line.

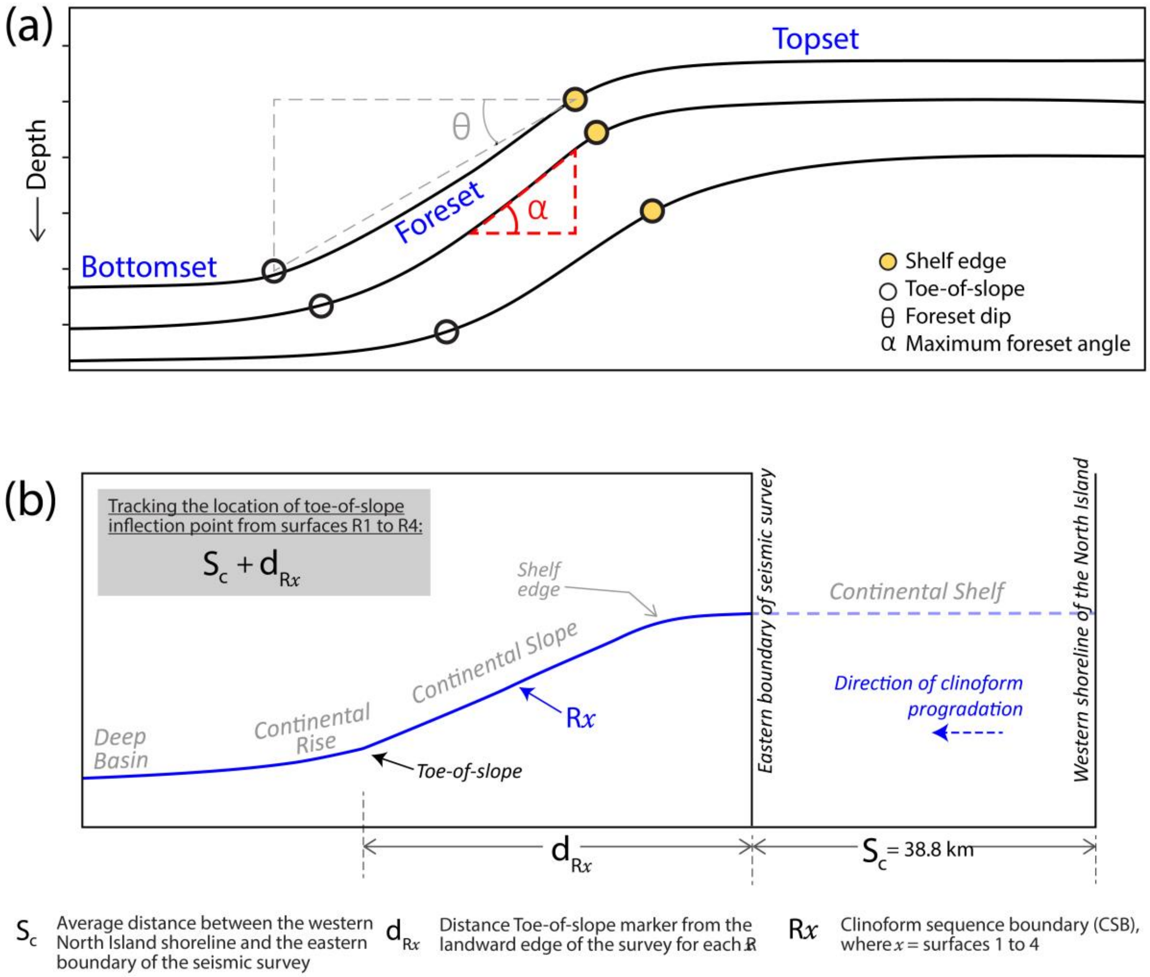

Figure 3. Measurement of the clinoform sequence boundary structure. (a) Schematic diagram illustrating the geometrical elements associated with progradational clinoform systems. We utilized the angular parameters α (maximum foreset angle, measured along the reflector surface) and θ (foreset dip, measured from the shelf edge to the toe of the slope) to quantify the clinoform geometries across the study area. (b) Schematic diagram showing the scheme used in this study to the track the migration of the continental margin over time. The average distance of the survey from the New Zealand cost is represented by the parameter S_c, and the distance of the toe of slope markeris represented by the parameter d_{Rx}. We evaluate the changes in the location of rise-basin transition over four clinoform sequence boundary surfaces (R1 to R4).

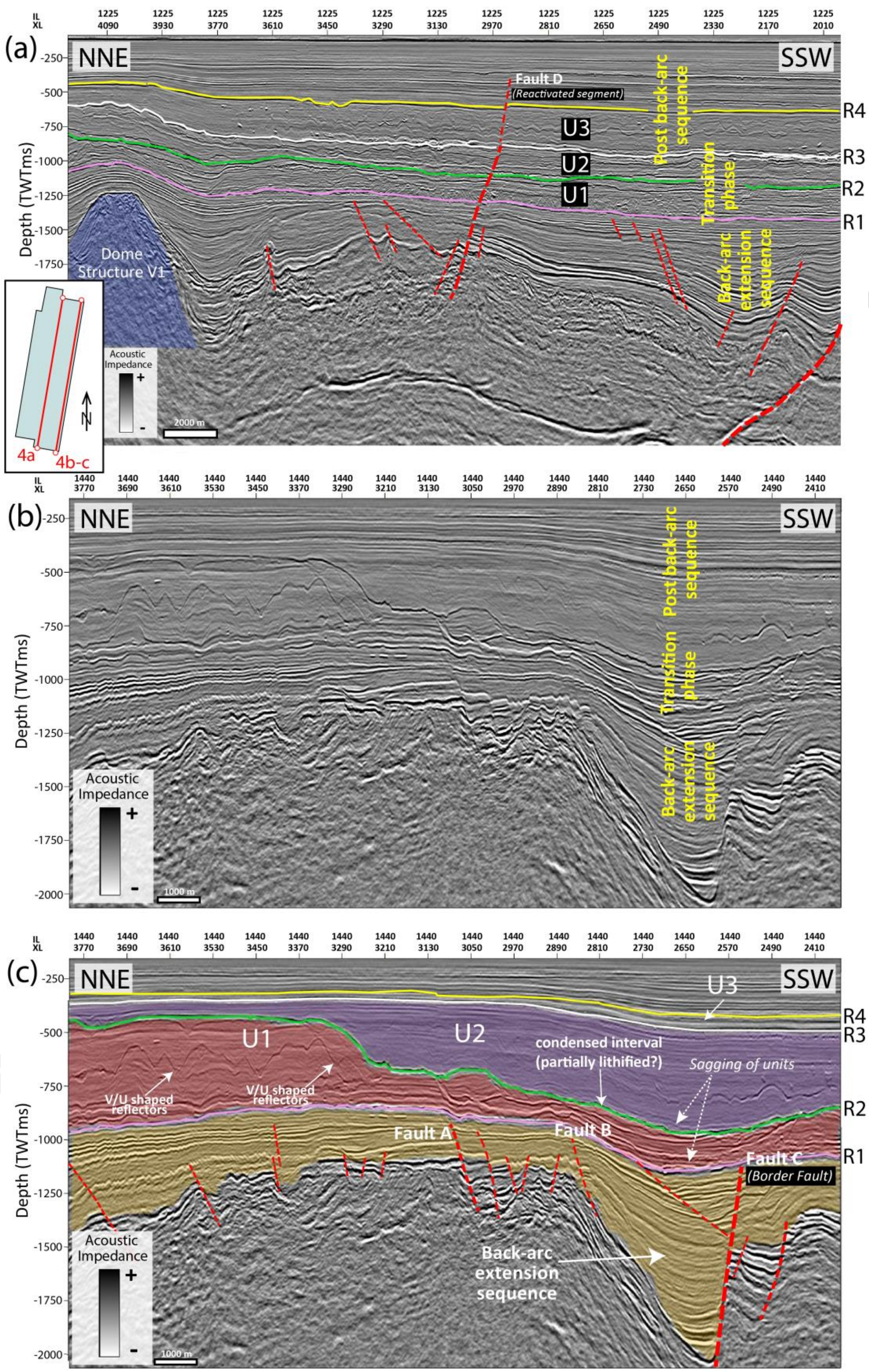
(a)
NNE
SSW
Fault D
(Reactivated segment)
U3
U2
U1
R4
R3
R2
R1
Post back-arc sequence
Transition phase
Back-arc extension sequence
Dome Structure V1
Depth (TWTms)
Acoustic Impedance
2000 m
4a
4b-c
(b)
NNE
SSW
Post back-arc sequence
Transition phase
Back-arc extension sequence
Depth (TWTms)
Acoustic Impedance
1000 m
(c)
NNE
SSW
U1
U2
U3
R4
R3
R2
R1
condensed interval
(partially lithified?)
Sagging of units
V/U shaped reflectors
V/U shaped reflectors
Fault A
Fault B
Fault C
(Border Fault)
Back-arc extension sequence
Depth (TWTms)
Acoustic Impedance
1000 m

Figure 4. Subsurface structure and sedimentary sequences. (a) Inline (IL 1225) cross-section across the survey showing a dome-shaped shaped structure within the back-arc interval (blue polygon). Units 1-3 are also interpreted, bounded by the horizons R1, R2, R3, and R4. (b) An uninterpreted inline (IL 1440) cross-section across the seismic survey. (c) Interpretation of the cross section in Fig. 5b showing the mapped horizons and the tectonic features that influence the shape of the progradaing sequences, together with V and U shaped reflectors. Colored polygons highlight the thickness of the units and the interpreted condensed section (surface R2). The sagging of the units in the central-south domain are potential results of differential compaction due to the underlain syn-rift sequence. See inset in Fig. 4a for the locations of the cross-section transects.

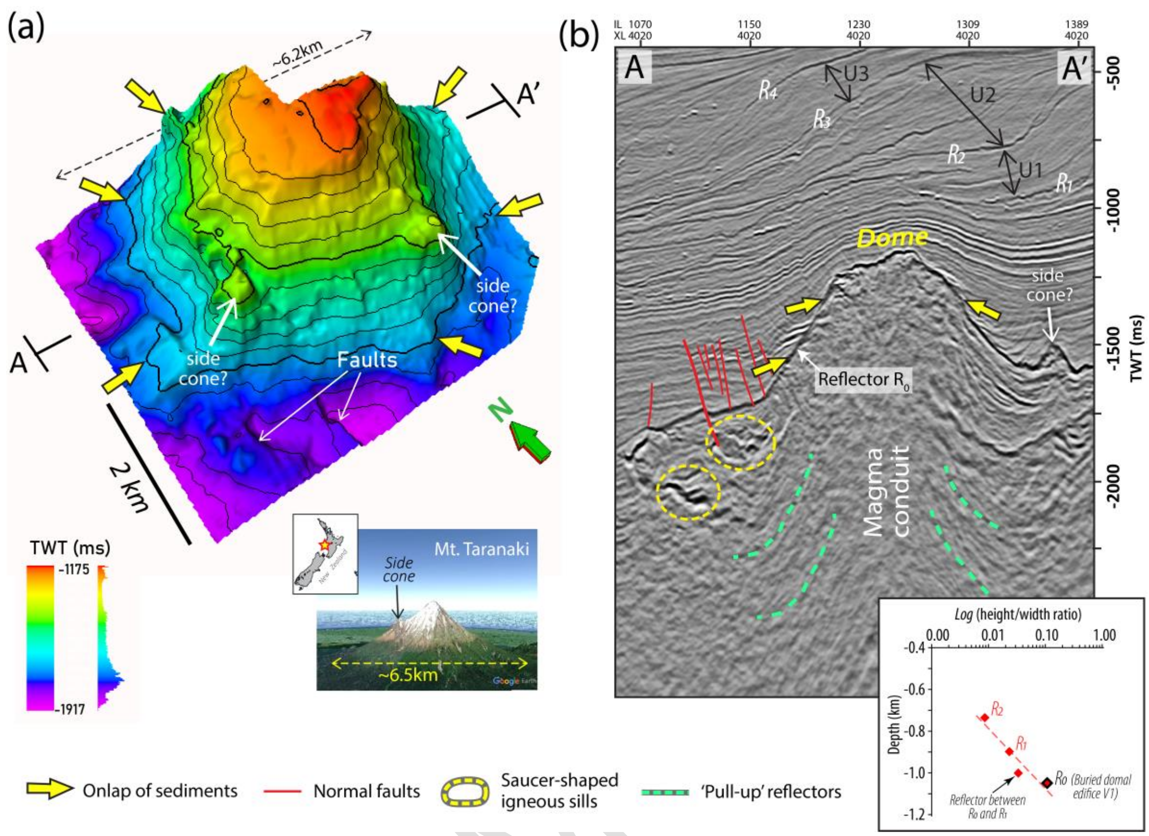

Figure 5. Miocene back-arc dome-shaped structures in the study area. (a) 3-D perspective view of the largest dome-shaped structure (Volcano V1 in Fig. 1b) in the northern part of the Nimitz seismic survey. We interpret the structure to be a volcanic edifice of the Mohakatino Volcanic Complex (MVC), with a diameter of ~6.2km, emplaced during the Miocene back-arc extension tectonics in the region. *Inset:* A modern day analogue, Mt. Taranaki, located further southeast of the study area, which is similar in dimensions to the intepreted dome shaped structures. (b) Crossline (XL 4020) seismic section showing the strong, high amplitude reflector associated with the top of the dome-shaped structures, the associated features at depth, and the distinct packages of prograding clinoforms at shallower depths above the dome structures. *Inset:* Plot showing a systematic (log-linear) variation of height/width ratio of buried seamount and overlying folds with shallowing depth.

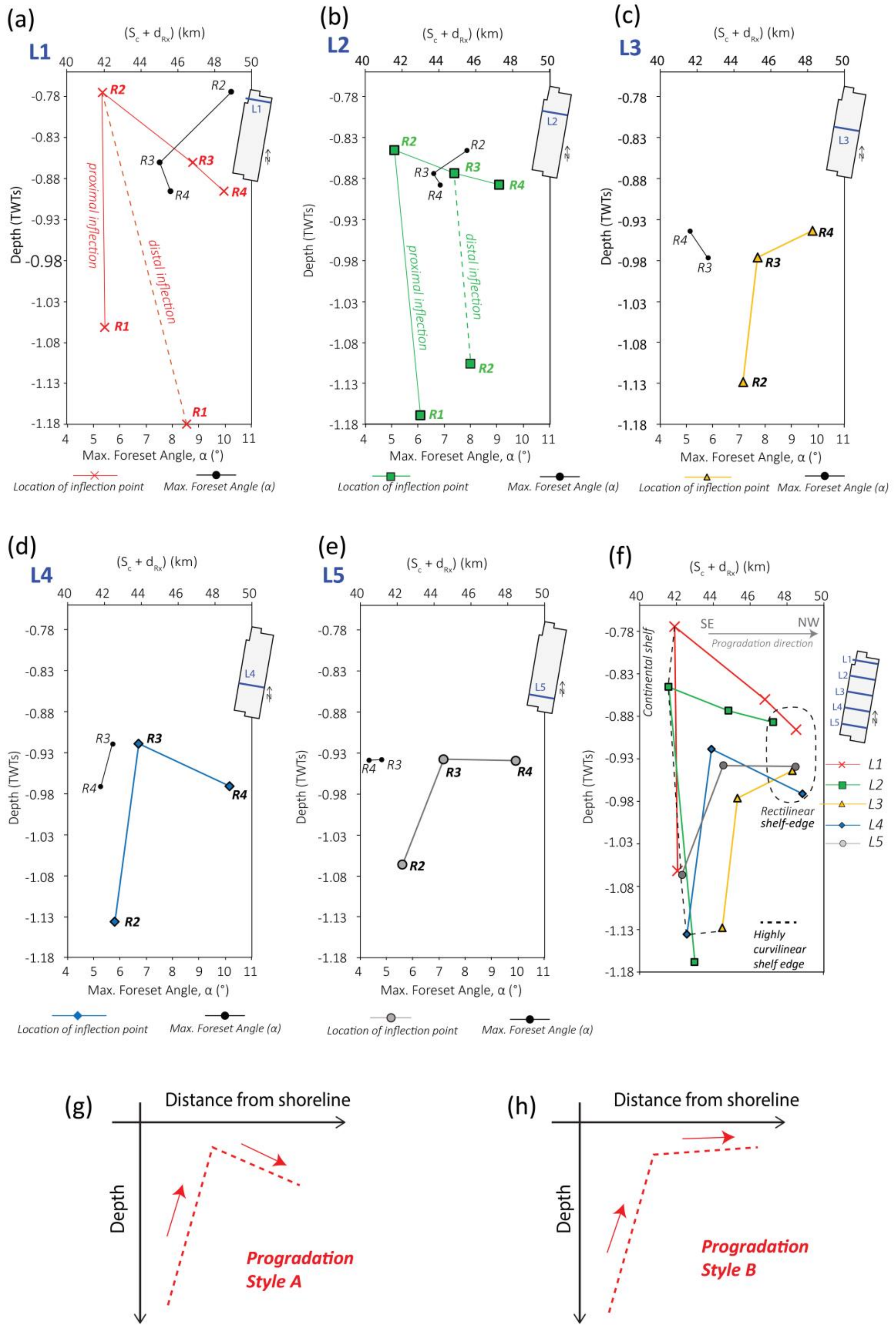
(a)
L1
(Sc + dRx) (km)
proximal inflection
distal inflection
Depth (TWTs)
Max. Foreset Angle, α (°)
Location of inflection point
Max. Foreset Angle (α)
(b)
L2
proximal inflection
distal inflection
(c)
L3
(d)
L4
(e)
L5
(f)
SE
NW
Progradation direction
Continental shelf
Rectilinear shelf-edge
Highly curvilinear shelf edge
L1
L2
L3
L4
L5
(g)
Distance from shoreline
Depth
Progradation Style A
(h)
Distance from shoreline
Depth
Progradation Style B

Figure 6. (a-e) Plots of depth (TWTTms) vs (S_c + d_{Rx}) for surfaces R1 to R4, measured in 6 km-spaced cross-sections L1-L5 along the survey. The plots are overlaid with the measured maximum foreset angle (α) on each section. The location of each of the profile transects is shown in the seismic survey map at the top-right corner of the plots. See Figure 3b for more details on the measured parameters. (f) Grouped plot depicting the changes in the strike oriented geometry and location of the shelf edge from surfaces R1 to R4. The clustering of the encircled-dashed points, represent the greatest uniformity of the prograding margin (and hence the shelf-edge) in relatively recent geologic time, and the connected dashed points, represent the highest curvilinear geometry of the prograding margin of a relatively older succession. (g-h) Two types of progradational styles (Progradational Style A and Progradation style B) based on the S_c+d_{Rx} versus depth (in time) trends observed in (a, b & d) and (c & e).

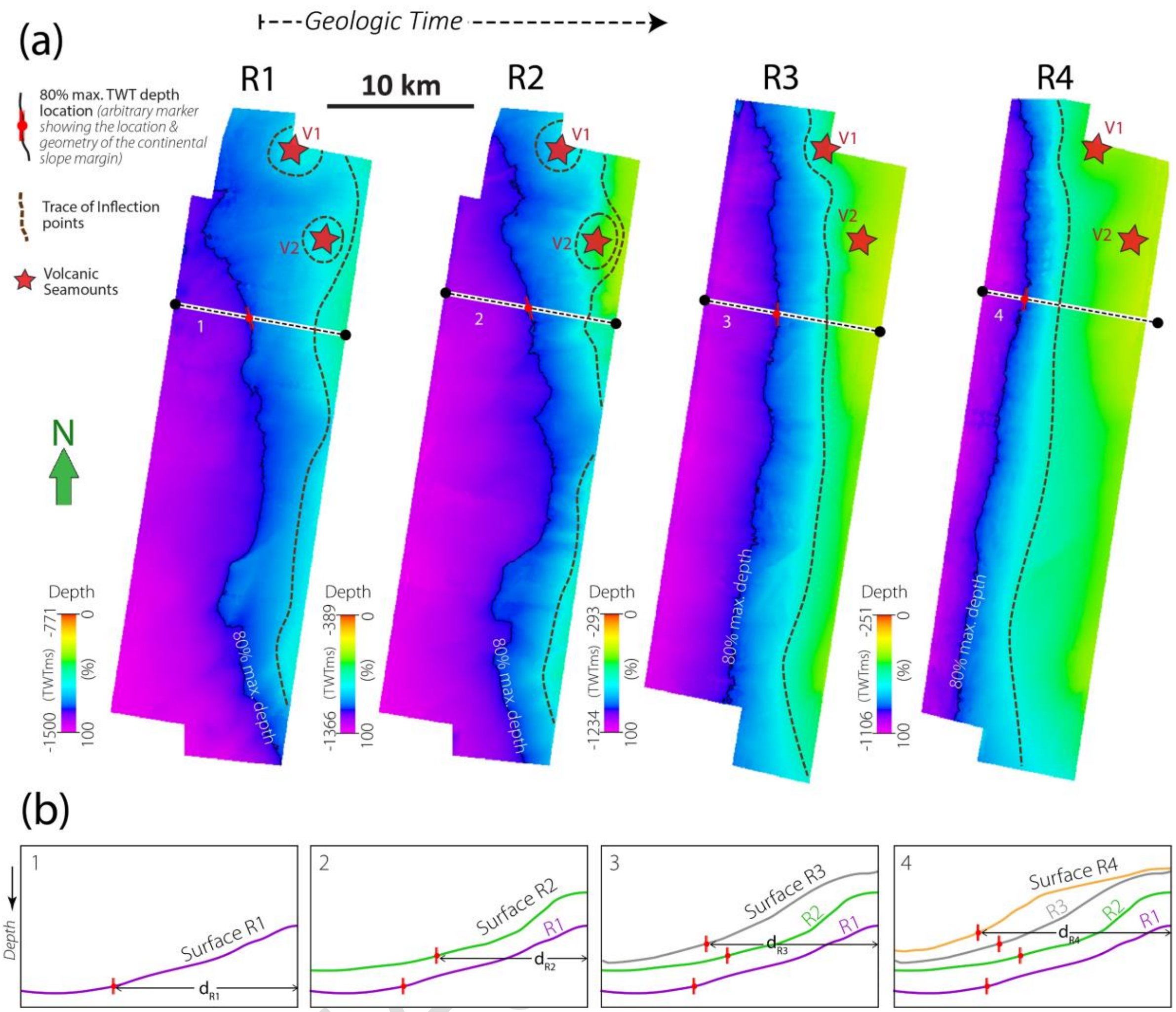

Figure 7. Spatio-temporal changes in the location and geometry of the Continental Slope Margin in the post-extension sequences. (a) Surfaces R1 to R4 showing the changes in the location and plan-view geometry of the toe-of-slope inflection across the survey. The surfaces are mapped on Two-Way-Travel time. The volcanic seamounts are located and tracked with respect to each surface (red stars). The influence of the volcanic edifices are most significant on the deeper horizon surfaces (R1 and R2). A max. depth contor line is used to further represent the geometry of the continental slope margin. (b) Representative interpretation cross-sections showing the migration toe-of-slope inflection point over time. See Figures 3b and 6a-f for more details on the quantification of the spatio-temporal location and geometry of the toe-of-slope inflection points.

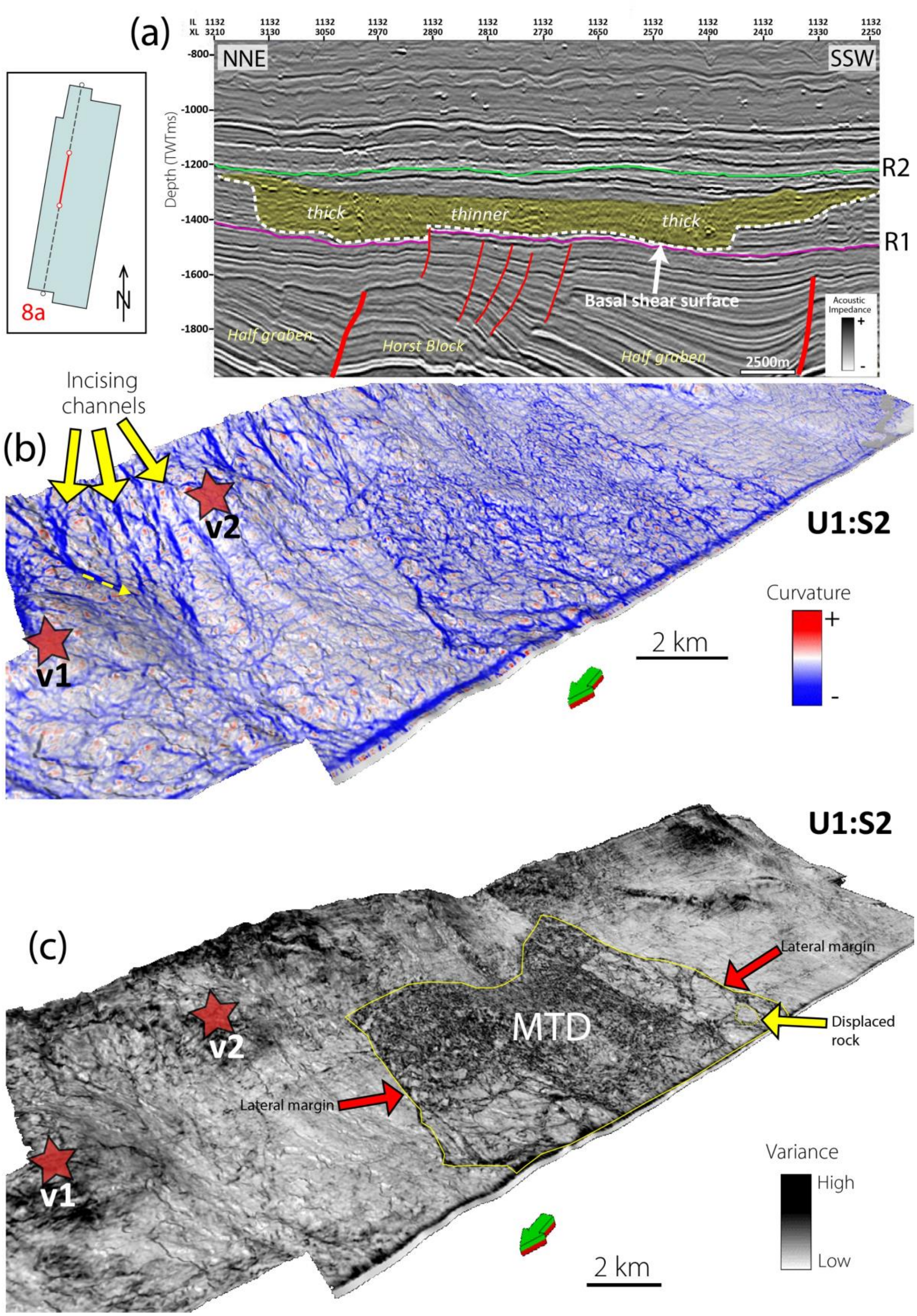
(a)
8a
N
NNE
SSW
Depth (TWTms)
R2
R1
thick
thinner
thick
Basal shear surface
Half graben
Horst Block
Half graben
2500m
Acoustic Impedance
(b)
Incising channels
v1
v2
U1:S2
Curvature
2 km
(c)
U1:S2
MTD
Lateral margin
Lateral margin
Displaced rock
v1
v2
Variance
High
Low
2 km

1428

Figure 8. Spatial distribution of progradational system elements in the post-rift sequences. (a) Cross-section showing a chaotic mid-high amplitude seismic package in the post-rift sequence (orange polygon), interpreted as a mass transport deposit (MTD) and its basal shear surface truncating continuous parallel reflectors. (b) Perspective view of a deeper surface (U1:S2) (See Figure 2c) within Unit-1 interpolated with the negative structural curvature attribute, revealing channel like features feeding into the basin. The yellow block-arrows show the convergent flow direction of closely spaced channels incising into an over-steepened slope in the northern domain, overlaying the location of the buried paleovolcanoes. The yellow-dashed arrow indicates SW flow of an incising channel feature over one of the two volcanic seamounts, eventually converging into a general westward direction (c) Perspective view of the same surface in Fig. 9b interpolated with the variance attribute, showing the MTD in the central part of the study area and its associated features. It is bounded by its lateral margins, and follows a northwest-westward erosional trend.

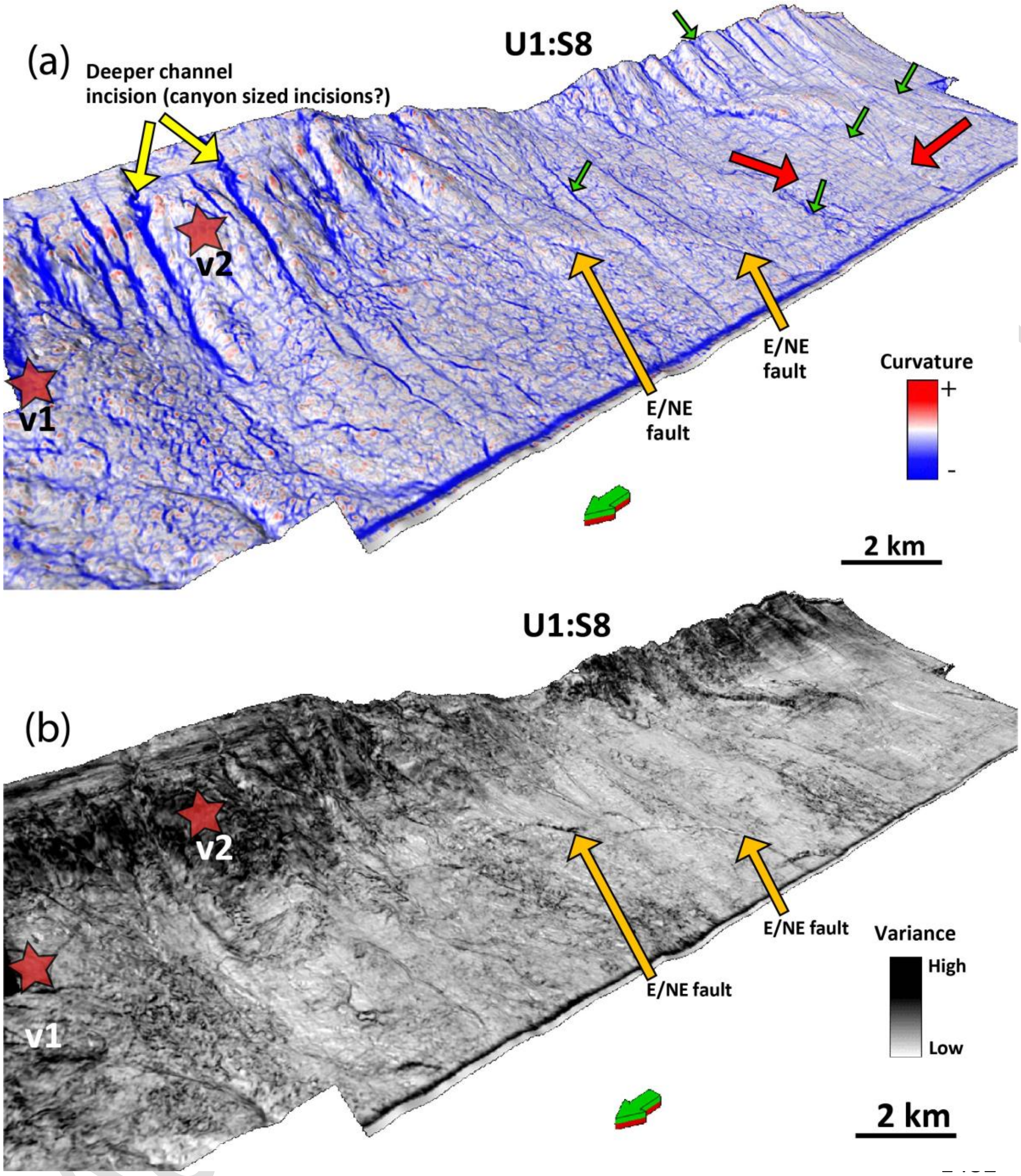

Figure 9. Perspective view from the NW, of a shallower surface within Unit-1 (S8) interpolated with (a) negative structural curvature, and (b) variance seismic attributes. The images show the dominance of wider incising channels, as compared to Fig. 8b along the shelf-edge and onto the continental slope within the northern domain of the seismic survey where the igneous bodies are located (red stars). Green arrows point and more channel like features in the central and southern domain, that are either linked to more submarine canyons or gullies. Red arrows point an area where the channels are difficult to interpret due to interpolation of the surfaces. It is however expected that the channels on upper slopes in the southern domain, migrate into the basin. Orange arrows point at an ENE-trending fault

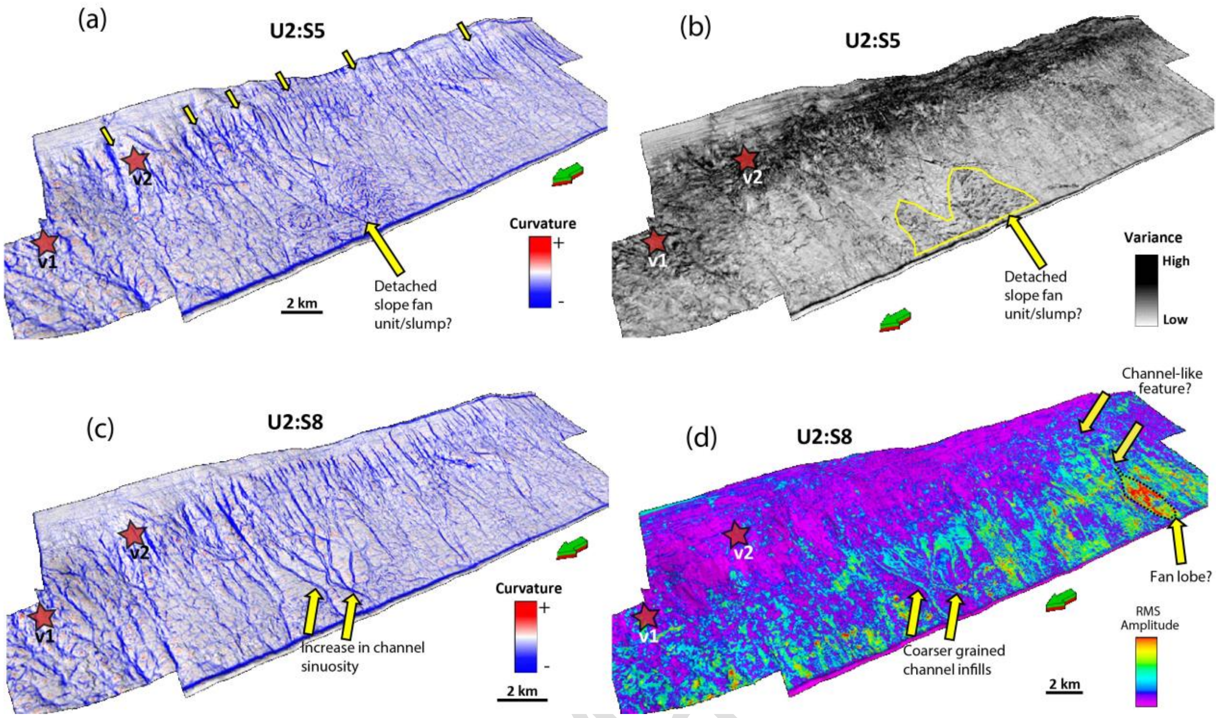

Figure 10. (a - b) Perspective views of an intermediate-depth surface within Unit-2 (S5) co-rendered with (a) curvature, and (b) coherence surface attributes. The yellow block arrows point to the increase in the frequency of submarine channels across the survey and a potential detached slope fan/slump in (a) & (b). (c – d) Perspective views of the shallower Unit-2 surface (S8), co-rendered with (a)negative structural-curvature, and (d) RMS Amplitude seismic attributes. (c) indicates the event of sinuous channel-like features and (d) highlights high RMS geometrically linear features of potentially coarser-grained channel infills and an interpreted submarine fan lobe with high anomalous RMS amplitude values.

1505

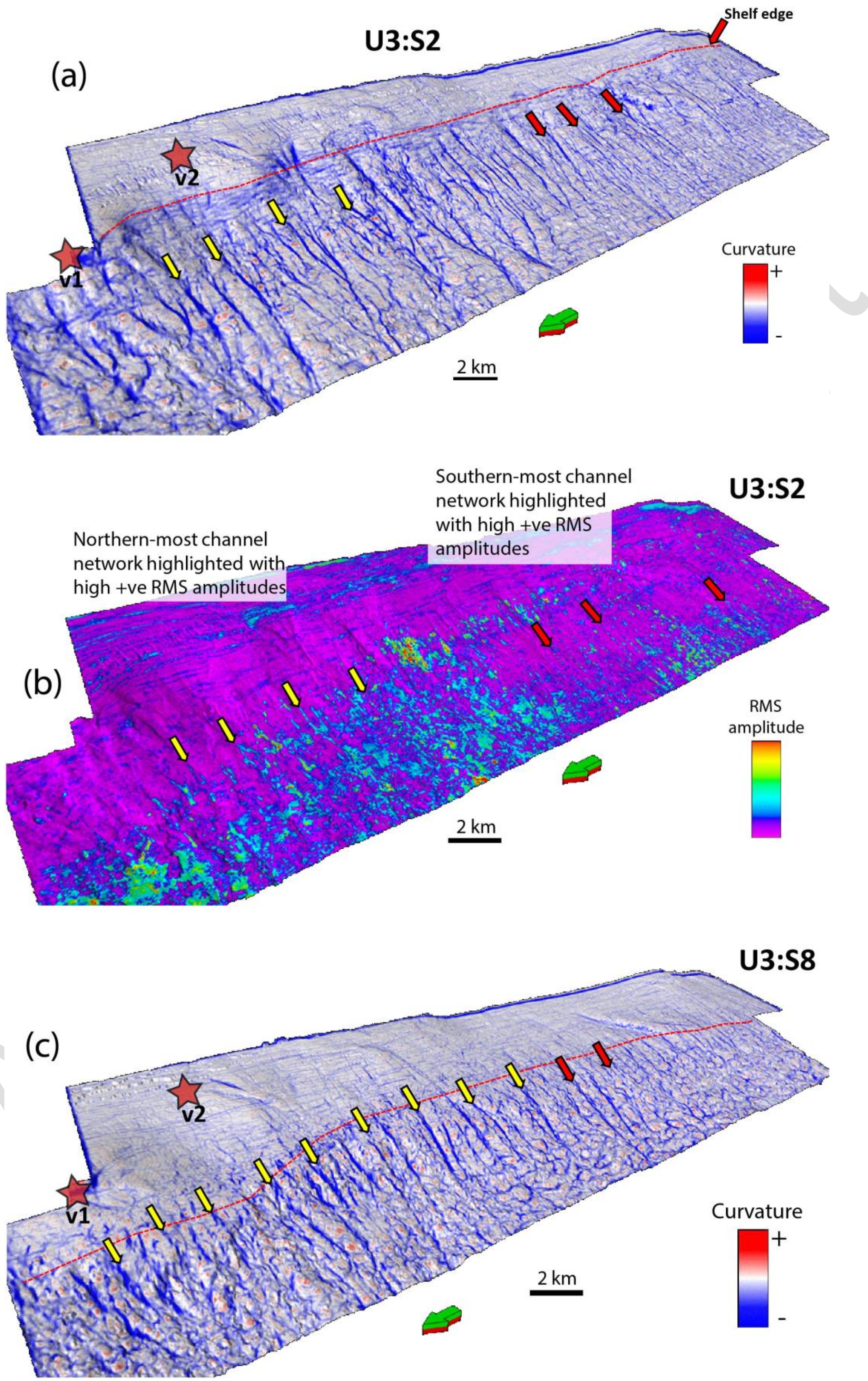

Shelf edge
U3:S2
(a)
v2
v1
Curvature
+
-
2 km
Southern-most channel network highlighted with high +ve RMS amplitudes
U3:S2
Northern-most channel network highlighted with high +ve RMS amplitudes
(b)
RMS amplitude
2 km
U3:S8
(c)
v2
v1
Curvature
+
-
2 km

Figure 11. (a – b) Perspective views of a deeper surface (S2) within Unit-3 co-rendered with (a) curvature, and (b) RMS Amplitude seismic attributes. The dashed-red line represents the location of the shelf-edge at that point in time. The yellow block arrows point to the increase in frequency of interpreted submarine gullies in the northern domain across the survey into the southern domain indicated by the red block arrows. The linear geometry of these submarine channel features is revealed by the high RMS amplitude values, and as aforementioned are likely filled with coarser grained sediment (c) Perspective of the shallower surface S8 within Unit-3 co-rendered with curvature attribute. Channel frequency continues to increase as the observed shelf edge migrates northwest/westward across the basin.

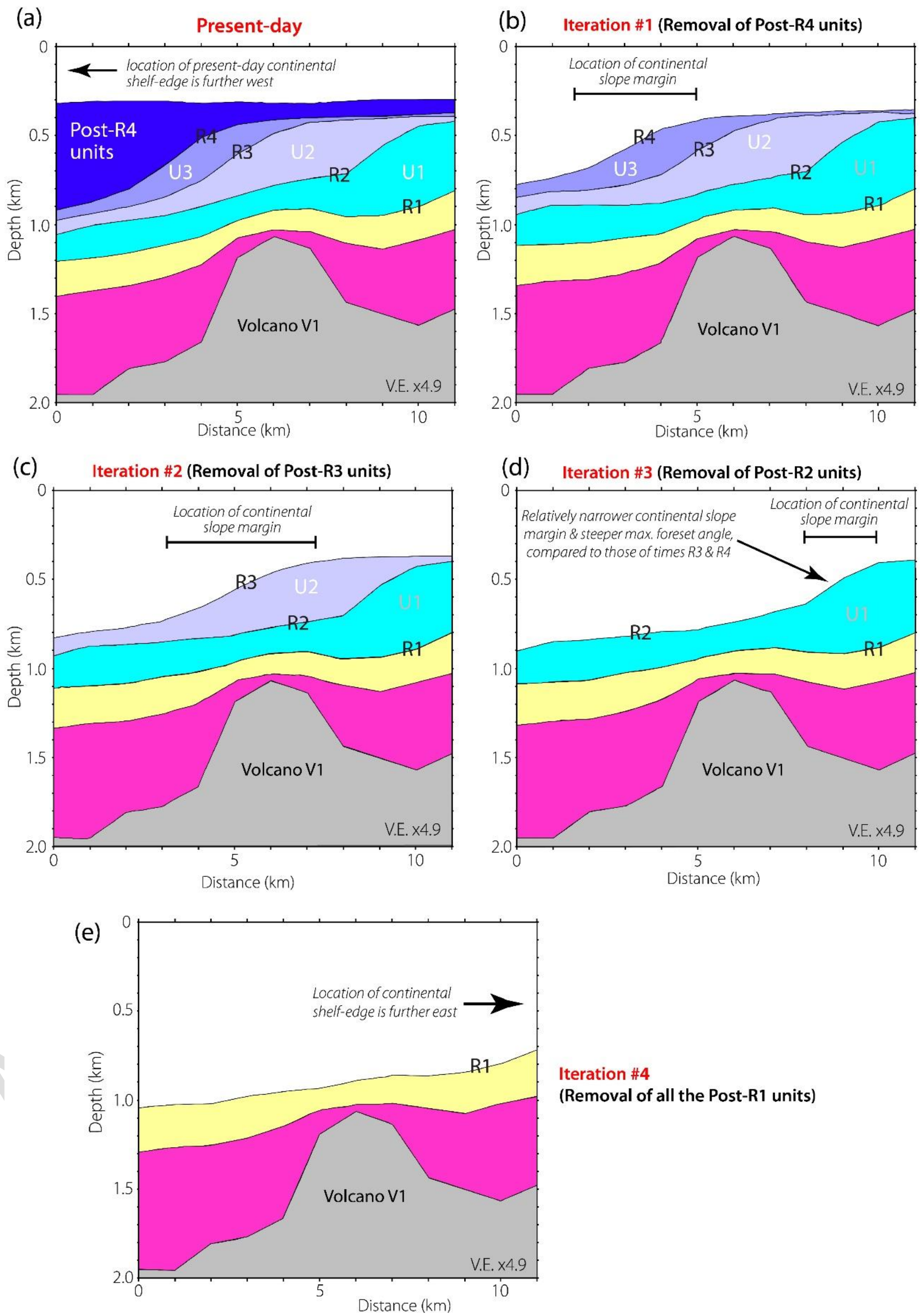
(a)
Present-day
location of present-day continental shelf-edge is further west
Post-R4 units
R4
R3
U3
U2
R2
U1
R1
Volcano V1
V.E. x4.9
Depth (km)
Distance (km)
(b)
Iteration #1 (Removal of Post-R4 units)
Location of continental slope margin
R4
R3
U2
U3
R2
U1
R1
Volcano V1
V.E. x4.9
Depth (km)
Distance (km)
(c)
Iteration #2 (Removal of Post-R3 units)
Location of continental slope margin
R3
U2
R2
U1
R1
Volcano V1
V.E. x4.9
Depth (km)
Distance (km)
(d)
Iteration #3 (Removal of Post-R2 units)
Relatively narrower continental slope margin & steeper max. foreset angle, compared to those of times R3 & R4
Location of continental slope margin
R2
U1
R1
Volcano V1
V.E. x4.9
Depth (km)
Distance (km)
(e)
Location of continental shelf-edge is further east
R1
Iteration #4
(Removal of all the Post-R1 units)
Volcano V1
V.E. x4.9
Depth (km)
Distance (km)

Figure 12. 2-D decompaction model of the northern domain. (a - e) Cross-sections showing the sequential decompaction models for each of the major clinoform packages of interest. The sections show that the most significant influence of differential compaction about the volcanic edifice occurred at Time R2, with minor influence at time R1 and R3 as well as the position of the migrating slope margin with time. See Figure S2 for depth converted seismic cross section that was used to generated the present day model seen in 12a.

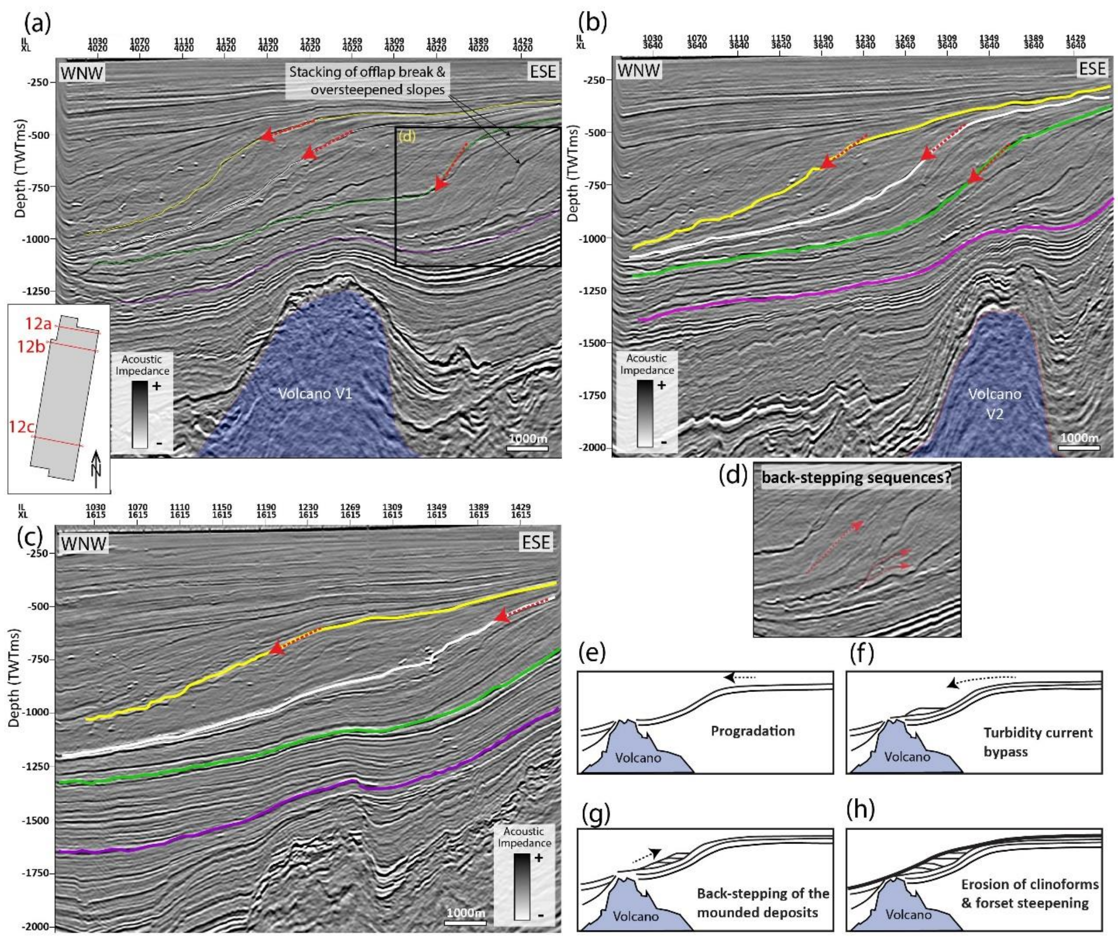

Figure 13. Buried volcanic massifs and the overlying post-rift sequences. (a - b) Cross-sections in the northern domain of the seismic survey, showing the stacking of the offlap breaks and oversteepening of the foreset slopes above the buried paleovolcanoes. Dominant oversteeping in observed in the older surfaces (R1-R2) primarily in (b). (c) Cross-section in the southern domain of the seismic survey showing clinoforms with gently dipping progradational clinoforms and little-to no disturbance of underlain volcanics. (d) Zoom-in of 13b, highlighting short, weak amplitude reflectors subparrelel to the clinoform surfaces, that may indicate backstepping seismic facies (e-f). Cartoons illustrating the interpreted mechanisms of clinoform development, the backstepping process and the effects of oversteepening of the shelf margin, imposed by a buried volcanic mound (after Johnston et al., 2010).

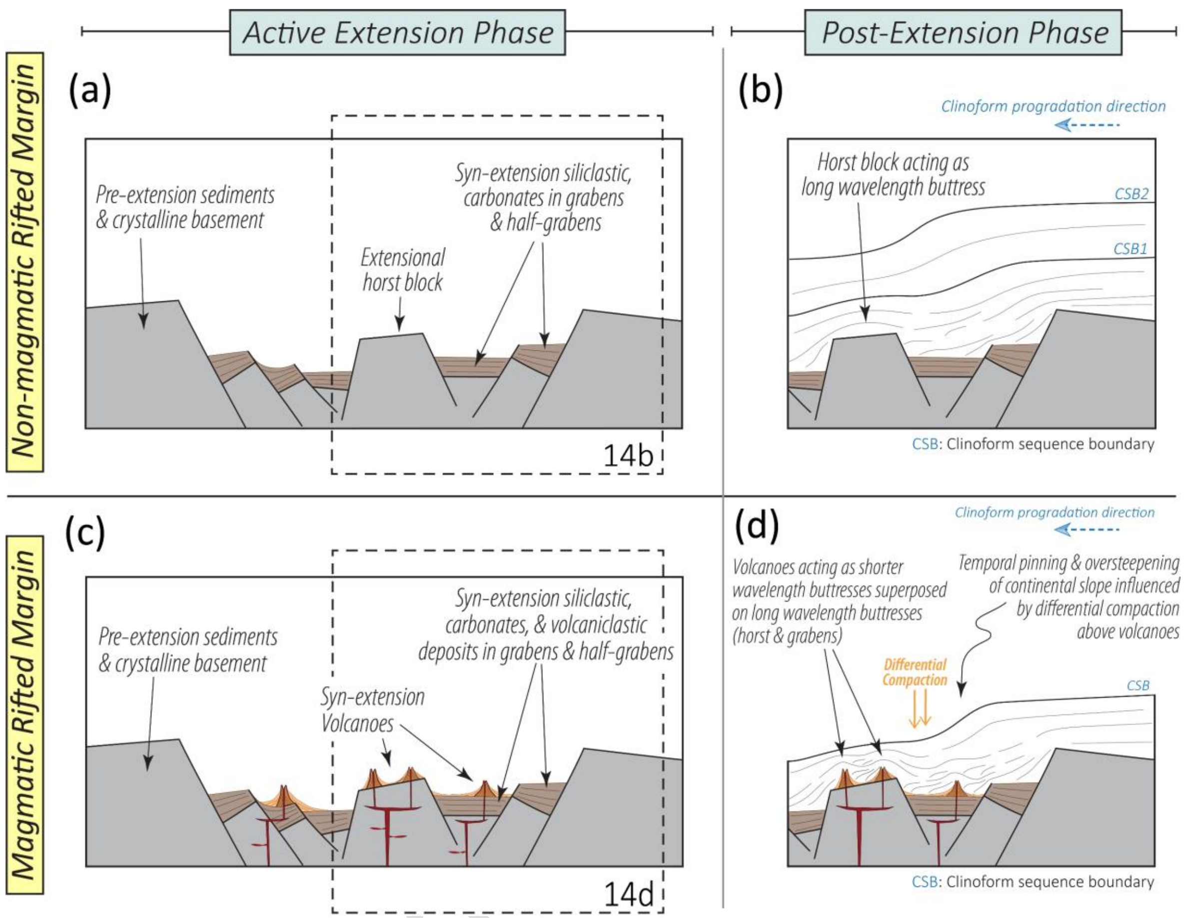

Figure 14. **Implications for magmatic and non-magmatic continental margins: Example of rifted margins.** Cartoon showing a conceptual comparison between the geometries of prograding sequences in post-extension phases within magmatic and non-magmatic rifted continental margins, with an emphasis on differential compaction influencing clinoform geometry above the volcanic mounds.